Winter 2014

Microscale and fluorescence-based techniques/ systems to monitor biological changes in real-time

Manasa Paidipalli
Louisiana Tech University

MICROSCALE AND FLUORESCENCE-BASED TECHNIQUES/ SYSTEMS TO MONITOR BIOLOGICAL CHANGES IN REAL-TIME

by

Manasa Paidipalli, B.Tech, M.S.

A Dissertation Presented in Partial Fulfillment
of the Requirements of the Degree
Doctor of Philosophy

COLLEGE OF ENGINEERING AND SCIENCE
LOUISIANA TECH UNIVERSITY

March 2014

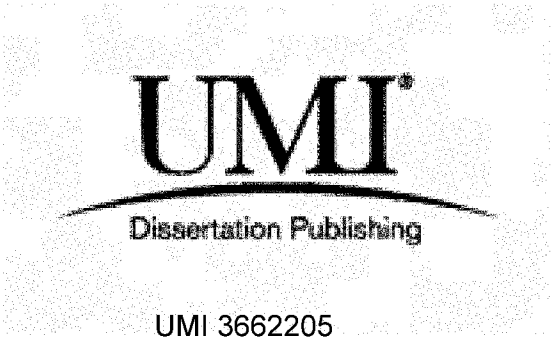

ProQuest LLC
789 East Eisenhower Parkway
P.O. Box 1346
Ann Arbor, MI 48106-1346

LOUISIANA TECH UNIVERSITY

THE GRADUATE SCHOOL

January 24, 2014

Date

We hereby recommend that the dissertation prepared under our supervision by Manasa Paidipalli, B.Tech, M.S.

entitled

Microscale and Fluorescence-based Techniques/Systems to Monitor Biological Changes in Real-time

be accepted in partial fulfillment of the requirements for the Degree of Doctor of Philosophy in Engineering

Supervisor of Dissertation Research

Head of Department

Engineering

Department

Recommendation concurred in:

Advisory Committee

Approved:

Director of Graduate Studies

Approved:

Dean of the Graduate School

Dean of the College

GS Form 13a
(6/07)

ABSTRACT

The long-term objective of this work is to develop an integrated continuous-flow microfluidic device for the analysis of genetic changes in DNA. Initially, this required the development of new techniques to simulate and then quantify DNA damage using existing laboratory instrumentation. Many analytical protocols exist for the quantification of varied types of DNA damage, which span a range of complexity and sensitivity. As an efficient alternative to the existing procedures, this work demonstrates the application of quantitative polymerase chain reaction (qPCR) and high-resolution DNA melting analysis (HRMA) to the detection and quantification of intramolecular DNA damage and/or strand breaks. These proven molecular biology methods are essentially single-step processes. When implemented with a third-generation saturating DNA dye, we have demonstrated that high sensitivity can be obtained with both qPCR and HRMA. This work reinforces the applicability of these techniques in the real-time analysis of biological changes using existing laboratory instrumentation.

In order to begin the next step of miniaturizing these protocols, we have refined a microfluidic fabrication protocol. Using these optimized processing conditions to manufacture prototype microfluidic devices, we have successfully achieved on-chip DNA amplification, which is the most critical component of the qPCR methods that we have developed for DNA damage analysis. By further integrating a fluorescence-imaging functionality into this system (which is beyond the scope of this current project), this

microfluidic system will provide a rapidity and sensitivity of DNA damage quantification that does not currently exist.

APPROVAL FOR SCHOLARLY DISSEMINATION

The author grants to the Prescott Memorial Library of Louisiana Tech University the right to reproduce, by appropriate methods, upon request, any or all portions of this Dissertation. It is understood that "proper request" consists of the agreement, on the part of the requesting party, that said reproduction is for his personal use and that subsequent reproduction will not occur without written approval of the author of this Dissertation. Further, any portions of the Dissertation used in books, papers, and other works must be appropriately referenced to this Dissertation.

Finally, the author of this Dissertation reserves the right to publish freely, in the literature, at any time, any or all portions of this Dissertation.

Author P. Hanara

Date 02/06/2014

DEDICATION

This work is dedicated to my loving parents, Krishna Rao and Nagamani Paidipalli, my husband, Karthik Ravi, and my brother and sister, Murali and Madhavi.

TABLE OF CONTENTS

LIST OF TABLES

LIST OF FIGURES

ACKNOWLEDGMENTS

I would like to express my sincere gratitude to my advisor Dr. Niel Crews for his guidance, encouragement and continuous support throughout the course of this accomplishment. Having an advisor like Dr. Crews has helped me gain insight in different fields of research, and he has been my source of inspiration since I joined the lab. I would also like to thank my committee members Dr. Guilbeau, Dr. Hindmarsh, Dr. Que, and Dr. Radadia for being a part of my advisory committee. I must especially thank Dr. Hindmarsh for the laboratory help and in-depth discussions held, which have guided me through the research.

I would like to extend my appreciation to all my family members, especially my uncle Babu Rao Paidipalli, for their love and support throughout my course of study. I can say it would have been impossible for me to achieve my goal without the complete support from Karthik especially after our marriage.

In addition, I would like to acknowledge my lab partners Ilija, Collin, James, and Varun for their helpful thoughts and discussions. I am thankful to all my friends who have showed great support through thick and thin, making my life pleasant and enjoyable.

CHAPTER 1

INTRODUCTION

In spite of the self-reparability of living cells, they are susceptible to various higher levels of damage when exposed to radiation, resulting in mutations and also cellular death. Radiation can either interact directly with the cellular components or indirectly with the water molecules inside the cells, thereby forming water-derived radicals [1-3]. Either way, radiation may cause short term or long-term consequences that would hinder cell functionality. The type of radiation-induced damage may occur in various forms such as: strand breaks, base damage, and inter-strand crosslinks [3, 4]. The severity of DNA damage is proportional to the time and intensity of radiation exposure.

1.1 Goal

The major goal of this project is to develop methods and tools for real time analysis of DNA damage when exposed to radiation. This includes experimental protocols for use on existing laboratory equipment, as well as the creation and validation of an integrated microfluidic system.

1.2 Hypothesis

Our hypothesis is that DNA damage in living cells can be quantified in real time using existing laboratory instrumentation and also in a micro-fabricated device, both of which are fluorescence-based systems. In an effort to prove our hypothesis, we have

quantified different types of DNA damage using a real-time instrument. Our aim is to show high sensitivity and also to demonstrate the capability of an integrated microfluidic system for the amplification of DNA.

1.3 Demonstration and Significance

We were able to demonstrate an efficient way of detecting different types of radiation damage in DNA in real time. These include intramolecular DNA damage, as well as strand breaks. We have developed fluorescence-based techniques for early DNA damage detection and also quantification of DNA damage using a commercially available real-time instrument. We have been able to amplify different targets in a DNA template in a single run in the real-time instrument. We have differentiated the damage caused from different types of UV radiation. We have been able to fabricate a microfluidic device, which along with a thermal and an optical set up was used to show on-chip quantitative Polymerase Chain Reaction (qPCR) and High Resolution Melting Analysis (HRMA). The microfluidic setup can be integrated further with a cell culture system, thus forming a stable microenvironment for cell growth and on-demand genetic analysis. The microfluidic system can thereby possess the ability for rapid and efficient detection of DNA damage.

DNA damage affects living cells in a number of ways. There is a clear need to combine different detection methods to quantify the damage and gain further insight into the related cellular disorders such as carcinogenesis and genomic instability. This thesis demonstrates the feasibility of damage analysis in living cells by using the microfluidic system such that the repair mechanisms can be studied with higher precision.

1.4 Background and Prior Work

1.4.1 Basics of DNA

Deoxyribonucleic acid (DNA) is the genetic material within the cell nucleus. DNA (Figure 1-1) is a polymer made up of four different types of nucleotides/bases called A (Adenine), T (Thymine), G (Guanine), and C (Cytosine). The backbone of DNA is a polymer consisting of sugar molecules with alternating phosphate groups. Two DNA strands running anti-parallel to each other are held together in a double helix structure with the help of complementary bases to form a double-stranded DNA molecule. The complementary base pair AT uses two hydrogen bonds, whereas GC uses three hydrogen bonds. This base pairing allows the GC pair to form a stronger bond compared to the AT pair.

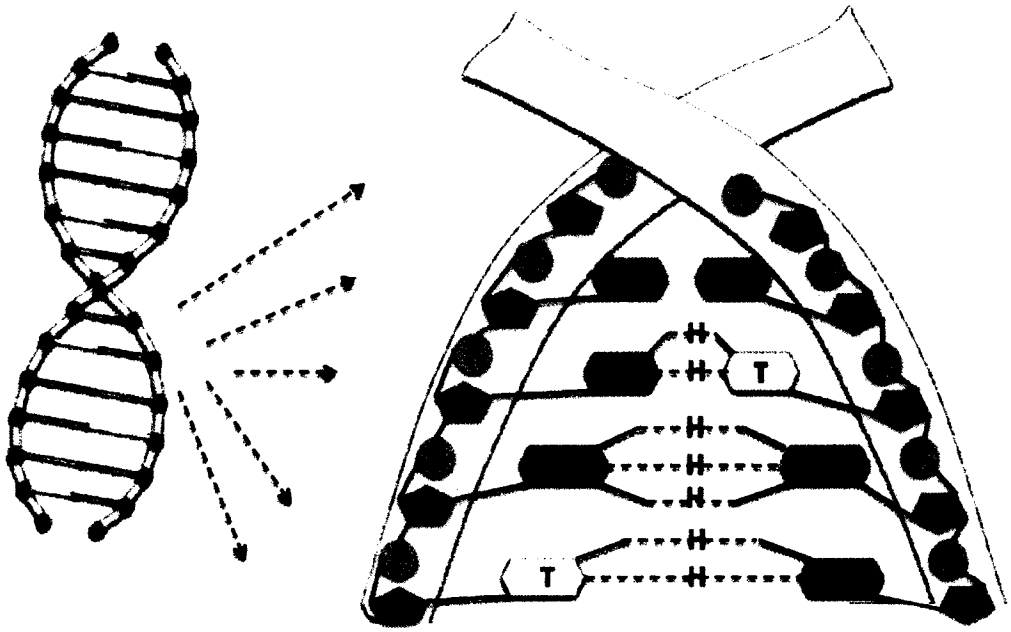

Figure 1-1: Structure of DNA.

1.4.2 DNA Amplification

Prior to cell division, DNA is replicated with the help of enzymes and proteins. The initial parent double-stranded DNA starts to unwind itself to form two separate single strands, onto which complementary bases are rearranged with the help of an enzyme called DNA polymerase, thus forming two double-stranded daughter strands. This process of DNA replication/amplification is synthesized in the laboratories by adding the necessary amounts of reagents to the initial DNA template. In the presence of sufficient reagents and the required temperatures, the DNA continues to amplify and is known as the Polymerase Chain Reaction (PCR). PCR is performed in multiple cycles of temperature changes consisting of denaturing step, annealing step, and an extension step. A double-stranded template converts to single-stranded at the denaturing step. Short strands of DNA called primers are bound to the ends of the single-stranded DNA at the annealing temperature. At the extension temperature, the complementary bases are polymerized all along the length of the single-stranded DNA, thus converting the two single-stranded DNA into two double-stranded DNA molecules. Multiple strands are thus formed from a double-stranded template DNA. The PCR technique was first developed for amplifying DNA in 1984 by Kary Mullis and has since then revolutionized areas including biological, medical, and clinical analyses [5]. PCR has become one of the most widely used techniques for nucleic acid analysis due to its high reproducibility and sensitivity [6].

1.4.3 qPCR and HRMA

qPCR is a PCR technique used to monitor the progression of the amplification and to determine the initial amount of DNA template present in the reaction mixture. A

dye is included in the PCR mixture and loaded into the real-time thermal cycler. In the thermal cycler, the dye exhibits fluorescence in the presence of double-stranded DNA, which shows the fluorescence signal to increase gradually with the number of PCR cycles. The proportional increase in the fluorescence intensity with the cycle number allows the quantification of DNA. A representative qPCR curve is shown in Figure 1-2. The cycle number (referred to mostly as C_p or C_T) where the amplification curve crosses the threshold and starts to give a fluorescence signal is a function of the DNA template concentration.

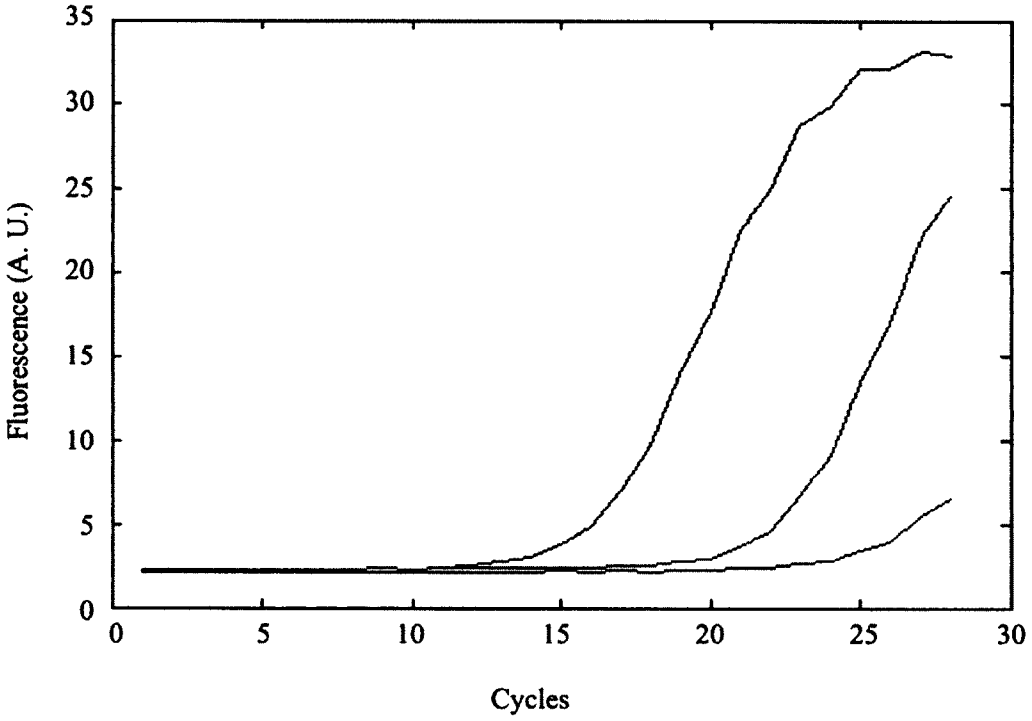

Figure 1-2: Sample qPCR amplification curves. The mixture with a higher initial DNA concentration (the leftmost curve in this example) starts to show fluorescence at an earlier cycle number.

The amplified DNA can further be analyzed in the real-time thermal cycler using HRMA, which is a rapid and cost-effective technique. In this technique, the sample is heated in a very controlled way up to and past the temperature at which the double-stranded DNA separates/melts. The initial double-stranded DNA therefore exhibits a high level of fluorescence that gradually decreases with an increase in the temperature. The first derivative of the resulting fluorescence versus temperature curve reveals the melting temperature [7] of the DNA, where 50% of the DNA is denatured. A representative graph of the DNA melting curve and its derivative plot is shown in Figure 1-3.

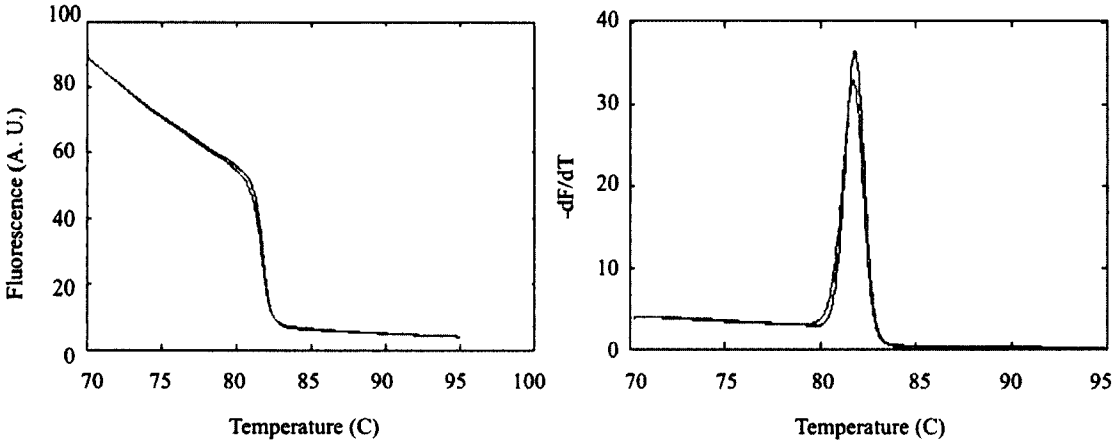

Figure 1-3: DNA melt curve and its derivative plot.

In the presented work, the real-time PCR instrument Light Scanner 32 (LS32) has been used for qPCR and subsequent HRMA on the samples. The subsequent HRMA on the PCR product is a measure of certainty that the fluorescence signal is from the actual product and not any non-specific amplification. The shape of the melting curves is a function of the sequence, length, and also the GC content [8]. When compared to the

conventional gel electrophoresis, HRMA can differentiate between different AT/GC ratio products having the same lengths.

1.4.4 DNA Damage

DNA damage can be a result of either daily activity in the cellular functioning or any external reacting agents. DNA damage can be caused through a wide variety of external factors such as ionizing and non-ionizing radiation, UV light, and also chemical agents such as hydrogen peroxide [3, 9, 10]. Table 1-1 summarizes a few different external agents capable of damaging DNA.

Table 1-1: DNA damaging agents.

Damaging agent	**Major damage detected**	**Detection methods**	**Reference**
UV-A radiation	• TT dimers • Oxidized bases	• High performance liquid chromatography-mass spectrometry (HPLC-MS) assay • Immuno-dot-blot assay	[1, 11-14]
UV-B radiation	• TT dimers • TC dimers • Photoproducts	• HPLC-MS assay • Immuno-dot-blot assay • PCR assay	[1, 12-16]
UV-C radiation	• TT dimers • Oxidative damage	• High performance liquid chromatography-electrochemical detection (HPLC-ECD) assay • Immuno-dot-blot assay • Electrochemical methods • qPCR assay • Long amplicon	[13, 16-21]

		qPCR assay	
Ionizing radiation	• Single-strand breaks • Double-strand breaks • Oxidative damage	• HPLC-ECD assay • Comet assay • Flow cytometry • Long amplicon qPCR assay	[2, 17, 21, 22]
Hydrogen Peroxide	• Base damage • Single-strand breaks	• Gas chromatography-mass spectrometry (GC-MS) • Comet assay	[9, 23, 24]

DNA when damaged may cause simple base changes or even complex alterations leading to mutations followed by cell death [4]. Since radiation exposure is one of the least understood of the damaging agents with DNA, in the presented work we have chosen to model DNA damage caused from radiation. The predominant forms of radiation damaged DNA are shown in Figure 1-4.

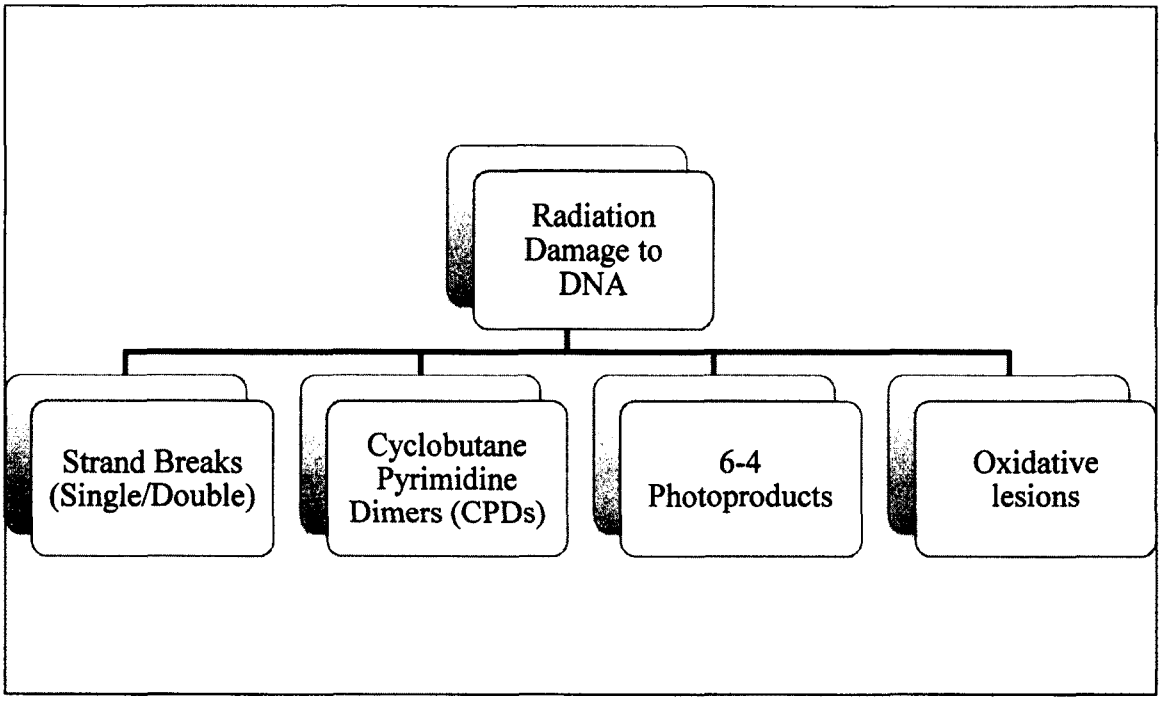

Figure 1-4: Major types of DNA damage.

Strand breaks, as the name suggests, are breaks produced either in a single strand (single-strand break) or in both the strands (double-strand break). Single-strand breaks can be produced directly by damaging agents or as intermediates in the process of repair [4]. Double-strand breaks are formed by ionizing radiation [4, 25] to a major extent even though formed with relatively lesser rate by non-ionizing radiation [11]. The coupling of the double bonds between adjacent pyrimidine bases forms CPDs [1]. Though occurring in less frequency when compared to CPDs, 6-4 photoproducts are considered to have more lethal effects when not repaired. The formation of 6-4 photoproducts involves the singlet-excited state caused by the coupling between the double bond of the pyrimidine and the carbonyl group [1, 22]. Oxidative damage to DNA is a result of photo-oxidation

reactions leading to products like hydroxyl radicals. Oxidative mechanisms are proven to be mutational and carcinogenic [1, 26].

1.4.5 Microfluidics

A dominant aspect of this thesis work deals with the improvement or acceleration of damage detection through the application of microfluidic technologies. Microfluidics deals with the manipulation and analysis of small amounts of fluids within the microchannels. This feature of miniaturization has applications ranging from industries such as biomedical, chemical, automotive and pharmaceutical to food and healthcare [5, 27]. Microfluidics, also known as micro total analysis systems or lab-on-a chip, gained traction in the 1990s, and since then it offers promising potential in the miniaturization of conventional equipment throughout academia and industry [28, 29]. The benefits of microfluidic systems include rapid analysis with short reaction times, high-throughput, handling small fluid volumes leading to low waste levels and less consumption of reagents, and lower cost.

1.4.6 Microfluidics for Biology

A variety of biological applications of microfluidics have been demonstrated including protein analysis, PCR amplification, and DNA sequencing. Microfluidics has been implemented towards integrated microfluidic PCR including micropumps, capillary electrophoresis and sample purification methods [6, 30, 31]. Conventional PCR would require a high consumption of reagents and also post-PCR analysis needs to be done off-line, making it difficult for integration onto the microsystems [5]. Research has been done to miniaturize thermo-cyclers to allow fast PCR cycle rates [30, 32]. Since the speed of PCR depends on faster temperature changes and heat transfer between the samples and

the device, rapid thermal cycling achieved through micro-fabricated PCR devices would be of great advantage. The added advantages of microfluidic devices include scope of parallel operation for multiple analyses and also the portability [32]. Integration of PCR with pre and post-amplification modules and also portable versions of these microfluidic devices have been reported [33] incorporating automated sample handling and also increased thermal response rate with a uniform temperature distribution [6].

1.4.7 On-Chip Microfluidics

The size of the microchannels defines the fluid flow in microfluidics to be laminar as shown by the Reynolds number R_e in Eq. 1.1:

$$R_e = \rho\mu D_h/\eta, \qquad \textbf{Eq. 1.1}$$

where ρ, μ, D_h and η are the density, flow velocity, hydraulic diameter and the dynamic viscosity in the microchannel, respectively. R_e is also referred to as the ratio of the inertial forces to the viscous forces as shown in Eq. 1.1. The small size of microchannels leading to a very low value of R_e thus indicates the dominance of viscous forces (η) when compared to the inertial forces ($\rho\mu D_h$).

Chip-based microfluidic PCR can be classified into well-based PCR [34-36] and continuous flow PCR [32, 37-39]. In well-based PCR, the sample inserted into the chip undergoes heating and cooling thermal cycles along with the chip which leads to larger thermal mass and longer cycling time. Continuous-flow PCR in turn uses fixed temperature zones through which the sample is flowed in order to attain the thermal cycling. The difference in the thermal cycling between the two approaches offers advantages to continuous-flow PCR in terms of rapid thermal cycling, less energy consumption, and ease of sample integration with other microsystems.

The initially developed continuous-flow PCR device by Nakano *et al.* [40] was capillary-based, which achieved a 50% amplification yield by using only 10% of the processing time compared to the commercial thermocyclers. Several other capillary-based devices were reported [41, 42]. In spite of the high amplification yield and speed, the difficulty lies in the integration of capillary-based devices.

A chip-based continuous-flow PCR device was first developed by Kopp *et al.* [39] in a Corning glass chip. This research group has reported on-chip amplification with a cycle time of 1 minute and the final PCR product was shown comparable to the commercial thermocyclers. Since then several groups have worked on the miniaturization and integration of the continuous-flow amplification systems and Table 1-2 gives a summary of the various continuous-flow PCR chips reported.

Table 1-2: Continuous-flow amplification systems reported [5, 43].

Layout	Heaters	Demonstration	Features	Reference
Fixed-loop with 20 cycles		Amplification of 176-base pair (bp) fragment in 90seconds	First on-chip continuous-flow PCR	[39]
Fixed-loop with 25 cycles	Integrated heaters	Amplification of 700-base pair (bp) fragment in less than 30 minutes	Proposed a liquid/liquid two phase PCR	[44]
Fixed-loop with 30 cycles	Integrated Indium-tin-oxide heaters	Amplification of 450-base pair (bp) fragment in 19 minutes	On-line fluorescence monitoring system	[45]
Fixed-loop with multiple cycles 20,		Amplification of 230-base pair (bp) fragment after	Integration of DNA and RNA amplification with cycle number	[46, 47]

25, 30, 35, and 40		30 cycles in only 6 minutes	selection; laser-induced fluorescence detection system	
Fixed-loop with 30 cycles	Integrated Indium-tin-oxide heaters	Amplification of 1460-base pair (bp) fragment in 60 minutes		[38]
Fixed-loop with 50 cycles		Amplification of 113-base pair (bp) fragment in 40 minutes	Prevention of air bubbles in microchannels; laser-induced fluorescence detection system	[48]
Fixed-loop with 20 cycles		Amplification of 632-base pair (bp) fragment in 14.6 minutes	Coupled with a solid-phase reversible immobilization chip	[37]
Fixed-loop with 20 cycles		Amplification of 90-base pair (bp) fragment	Numerical simulation for device optimal design; Reduced transition time between the temperature zones	[49]
Closed-loop design		Amplification of 500-base pair (bp) fragment in 13.5 minutes	Magnetohydrodynamic force used to pump fluid	[50]
Fixed-loop with 30 cycles		Amplification of 290-base pair (bp) fragment in 18.7 minutes	Coupled with 13 cycles for an allele-specific ligation detection reaction	[51]
Oscillatory PCR chip		Demonstrated to determine the threshold cycle number for their device	Proposed a parallel design to increase throughput; On-line optical detection system to monitor fluorescence level	[52]
Fixed-loop with 40 cycles	Integrated heating/cooling elements	Amplification of 108-base pair (bp) fragment in less than 9 minutes	Narrowing/widening channels to manipulate temperature gradient; resulted in smaller device footprint	[43]

On-chip continuous-flow PCR does suffer from a few limitations such as the generation of air bubbles in the microchannels, lack of flexibility in controlling the flow velocity regionally as per the PCR requirements, and a pressure-driven flow requiring an external syringe pump. However, a few alternative approaches have been developed to overcome the above issues. The generation of air bubbles has been addressed by having a fluorinated oil cap just ahead of the PCR sample into the microchannels [48]. Regional velocity control in the microchannels with an improved heating configuration has been reported for an efficient on-chip PCR [49]. The requirement of an external pump can be eliminated by the use of an electro-osmotic flow driven PCR [53-55].

PCR requiring smaller volumes helps to reduce costs and also enables rapid thermal cycling but may not reduce the amplification time needed if an efficient heater assembly is not used. The thermal mass of the system thus plays a crucial role in the speed of the PCR [56]. Table 1-3 presents on-chip continuous-flow PCR experiments and the parameters used by different research groups.

Table 1-3: Chip-based continuous-flow amplification [56].

Reaction volume (nl)	**Amplicon length (bp)**	**Amplification time (s)**	**Amplification cycle number**	**Time per cycle (seconds/cycle)**
100	430	480~1800	30	
500	500	1086	27	~40
1000		~900	35	~26
~6000	145	2100	25	84
4500	240	2280	23	~12
8000	372	300	40	7.5

1.4.7.1 *Materials for Microfabrication*

The first material used for microfluidics was silicon, followed by glass [29, 56-58]. Recently, the use of elastomers such as polydimethylsiloxane (PDMS), polymethylmethacrylate (PMMA) and polycarbonate as alternative substrates has increased [56, 58]. Commonly used methods for the fabrication of microfluidic devices include wet or dry etching, reactive ion etching, photolithography, soft lithography, laser ablation, hot embossing, and xurography [29, 30, 59].

Each of the substrates is associated with several advantages and disadvantages and therefore the appropriate substrate is chosen based on factors such as desired application, available technology and cost associated. The high thermal conductivity of silicon ensures a uniform temperature distribution and thus rapid thermal cycling. However, silicon is not compatible with PCR; its thermal conductivity causes problems with thermal insulation; its electrical conductivity creates problems in integration; its optical opacity in visible light is a limitation [29, 56-58]. Glass devices are beneficial in terms of mechanical strength, optical properties, biological sample compatibility, gas impermeability, relatively low nonspecific adsorption and well-known surface chemistry [29, 30, 58]. However, the higher costs, material and energy requirements in silicon and glass processing have led to the investigation of disposable microfluidic devices made out of polymers. Being an inexpensive elastomeric polymer, PDMS possesses several advantages such as flexibility, simplifying formation of multi-layer devices, better optical transparency, higher biocompatibility than silicon, and also ease of integration with on-chip fluidic pumps/valves [56, 57]. However, the low thermal conductivity of all optically-clear polymers is a severe disadvantage, particularly for continuous-flow

systems. The presented work deals with fabrication of glass micro devices owing to their optical and thermal properties necessary for on-chip PCR and fluorescence based detection.

1.4.7.2 *Surface Treatment of Microchannels*

The high surface-to-volume ratio in the microchannels causes problems with the PCR mixture flow. The irregularities inside the fabricated channels such as surface roughness limit the PCR efficiency by increasing the possibility of interaction/adsorption of the biomolecules with the channel walls. This suggests the need for surface modification/treatment for the operation of on-chip PCR. Different techniques for surface modification have been investigated and can be classified into static and dynamic treatment [6, 28, 32, 56, 60, 61]. Static treatment refers to the pre-coating of the surface during fabrication or just before chip use with materials such as silicon dioxide, silanizing agents, polymer coatings, and bovine serum albumin (BSA) [6, 56, 60]. Surface modification of PDMS from hydrophobic to hydrophilic has been possible through oxygen plasma treatment [32, 56]. Dynamic coatings of channels using SigmaCote (Sigma-Aldrich, USA) silanization methods have also been investigated [62]. The other widely used dynamic reagents include BSA, polyvinylpyrrolidone (PVP), polyethylene glycol (PEG) and Tween 20 [6, 32, 44, 56]. BSA and Tween 20 when added optimally can improve the PCR efficiency by decreasing the adsorption of the DNA polymerase [44, 56].

1.4.7.3 *DNA Detection Methods*

Several DNA detection methods have been investigated both off-line and also on-chip. Off-line detection techniques use intercalating dyes such as SYBR green, LCGreen

plus and RDT-D1 in combination with gel electrophoresis to detect the post amplification products [31, 56]. A few other off-line detection techniques include flow cytometry [63-65] and electrophoresis systems [66-68]. However, the off-line techniques are time-consuming and have an increased risk of contamination during the sample loading process.

On-chip detection methods can be optical, electrochemical or mass spectrometry detection. Optical detection methods were the most commonly used due to the advantages such as good detection limits, reasonable equipment requirements, isolation from the sample, and ease of implementation [29, 30]. Fluorescence-based detection methods are widely used in detection due to their sensitivity. Off-chip fluorescence typically uses a laser excitation source with charge-couple device (CCD) cameras or a photomultiplier to detect the fluorescence [29, 30]. With the increasing popularity of fluorescence-based detection, labeling or intercalating dyes have been developed. Real-time DNA detection has been developed based on the fluorescence emitted from the interaction of the dyes with the increased amount of double-stranded DNA after amplification. The end-point analysis is obtained by measuring the sample fluorescence before and after amplification, which is an indication of the amplified double-stranded DNA. In addition to fluorescence, chemiluminescence (production of light through a chemical reaction) and UV absorbance detection methods are also used in microfluidics [29, 30].

1.5 Roadmap

The experimental design and the various steps undertaken to achieve the goal of this project have been summarized in the following chapters. Chapter 2 focuses on

different types of simulated DNA damage and its detection by applying qPCR and HRMA techniques on the real-time PCR instrument LS32. It also discusses different analyses performed using LS32. Most of the results presented in this chapter have been published in the Journal of Microbiological Methods [69]. Chapter 3 discusses the fabrication materials and procedures used in the fabrication of the microfluidic device. It also covers the complete experimental set-up of the microfluidic system including the microchip, heating assembly, optics, and the pumping system. The results of the on-chip microfluidic PCR have been presented. Chapter 4 discusses the conclusions and the direction of future work. It also highlights the differences between the conventional instrumentation and the microfluidic system.

CHAPTER 2

EXPERIMENTS ON CONVENTIONAL INSTRUMENTATION

2.1 Background

DNA in vitro and in vivo is prone to damage when exposed to high-energy radiation [1]. This damage can be a breaking of one or both of the strands in the DNA helix, a fusing of the two strands to each other, to themselves (dimers), or other types of molecular damage to the nucleotides. Fragmented DNA can be observed directly using conventional techniques such as capillary electrophoresis [70] and the comet assay [71]. The observation of internal damage has typically required more circuitous analysis, such as high performance liquid chromatographic-mass spectrometry (HPLC-MS/MS) [16], hydrolysis of DNA followed by chromatographic separation [17], electrochemical measurements [18], or the enzymatic conversion of photoproducts into strand breaks [16].

This chapter reports the use of intercalating dye strategies to directly detect strand breaks as well as intramolecular damage of DNA by means of qPCR and/or HRMA in the LS32. This chapter also discusses the use of the real-time PCR instrument not only for multiplex amplification and detection of samples (two different amplification products being distinguished in a single tube), but also detection of damaged DNA in multiplexed samples. Being cost-effective, detection of real-time multiplex PCR damage also proves to be advantageous in terms of time needed for distinguishing different

products. The techniques demonstrated here provide a wide range of applications within the field of microbiological sciences. For example, the qPCR method could be used to determine the relative resistance of genes of interest to different damage mechanisms, or the qPCR and/or the HRMA technique could be used to evaluate the effectiveness of sterilization techniques for medical tools [72], food processing [73, 74], industrial cleanroom environments [75], and to detect food-borne pathogens such as Escherichia coli [76], and Brucella species [77], clinical laboratories for diagnosing multiple viruses [78].

2.1.1 qPCR

An intercalating DNA dye added with other reagents used for DNA amplification performs quantitative PCR. This particular family of dyes exhibits an increase in fluorescence emission when in the presence of double-stranded DNA (dsDNA). As the concentration of amplicon increases with each successive PCR cycle, the increase in the fluorescence intensity reveals the real-time kinetics of the amplification. This is used to determine the initial concentration of DNA in a given PCR mixture [79]. Neither internal damage (e.g. photoproducts) nor external damage (e.g. double-strand breaks) produces change in the initial DNA concentration. However, it does reduce the amount of amplifiable DNA in the sample [80, 81]. This equates to an effectual reduction in the initial DNA concentration, which can be measured by qPCR. In this way, the rapid processing and high sensitivity of qPCR can be used to quantify DNA damage. This technique can be applicable not only to quantify the damage to DNA, but also in various fields of genetic engineering [82], environmental detection, and quantification of

microorganisms such as airborne Thermoactinomyces vulgaris [7], E. coli [83, 84], and thermophilic bacilli in milk powder [85].

2.1.2 HRMA

High-resolution DNA melting analysis is commonly used as a label-free fluorescence technique for DNA genotyping and mutation scanning [86, 87], and it is sensitive enough to distinguish even single-base changes to a DNA sequence [88]. Other applications of HRMA include pre-sequence screening, variant fraction quantification, methylation studies [89], detection of mutations in Plasmodium falciparum genes related to malarial drug resistance [90], and diagnosis of cryptosporidiosis, an intestinal disease in humans [91]. HRMA is performed on a concentrated DNA mixture containing an intercalating dye (such as qPCR amplicon) by observing the fluorescence decay as the sample is heated above its melting temperature. As the DNA denatures, the fluorescence decreases as a function of strand separation. Maximum sensitivity is obtained when a saturating intercalating dye is used [92]. HRMA is perfectly compatible with qPCR amplification, and it can be performed as an endpoint analysis in several commercially available PCR instruments [93]. For complex HRMA data sets, the melt curves can be deconvoluted into critical parameters [94]. At its essence, HRMA is simply a measure of the binding energy between the DNA strands. "DNA melting" occurs when the thermal energy provided by the increasing temperature exceeds the binding energy between the two strands of DNA. The hydrogen bonds are then broken and the strands dissociate. Any change in the overall or local binding energy will change the behavior of the melt. This produces a shifting and/or shape change of the fluorescence versus the temperature DNA melting curve. Even more than the melt curve itself, the slope of the melt curve as a

function of temperature (called the derivative plot) highlights differences between the samples. This allows HRMA to reveal any quantitative and qualitative changes in the DNA samples. Because damaged DNA has a lower total binding energy, degrees of damage can be monitored with HRMA. This chapter demonstrates the use of qPCR and HRMA to monitor biological changes in real-time. To model intramolecular DNA damage, UV-C was used to induce cyclobutane pyrimidine dimers (CPDs) in the DNA [95]. To model double-strand breaks (DSBs), a restriction enzyme was used to cleave DNA. To detect multiplex PCR damage using qPCR and HRMA, two different primer sets have been added to the master mix along with the other PCR reagents. A variety of plasmid templates and amplicon targets were used for experiments presented in this chapter.

2.2 Experimental Materials and Methods

2.2.1 Procedures

2.2.1.1 *PCR*

The PCR mixture was prepared with DNA template, 0.5 mM of each of the forward and reverse primers, 200 mM of each deoxynucleotide triphosphate (dNTP), 0.08 U/μL of KlenTaq1 polymerase (AB Peptides, MO, USA), 0.08 U/μL Monoclonal Anti-Taq Antibody (eEnzyme, MD, USA), and 3 mM MgCl2 in a 50 mM Tris (pH 8.3) buffer. The mixture included 1 X of a third generation saturating dye (LCGreen Plus, BioFire Diagnostics, Inc., UT, USA) optimized for the real-time PCR instrument (LS32, BioFire Diagnostics, Inc., USA) and sample glass capillaries (LightCycler® Capillaries, Roche) used in these experiments. Reaction volumes of 10 μl were used for all PCR tests. Up to 32 samples were simultaneously amplified in accordance with the manufacturer's

instructions and known rapid PCR protocols [96]. The parameters of the amplification protocol (cycle number and the denaturing, annealing, and extension temperatures) were optimized for each template/primer combination used. For all PCR experiments, the hold times at each temperature were: 3 s – denaturing, 3 s – annealing, and 3 s – extension. The ramp rate between each temperature was 5°C/s.

2.2.1.2 *DNA Damage*

Damage by UV irradiation (creating CPDs) was performed by exposing DNA samples in a UV-C crosslinker (CL-1000, UVP, CA, USA), having five 8 W UV-C bulbs (G8T5, Sanyo Denki America, Inc., CA, USA) with an emission wavelength of 254±2 nm. For other experiments, DSBs were formed by digesting PCR-amplified DNA using the CaC8I restriction endonuclease (New England Biolabs, MA, USA). The digestion was performed in accordance with the vendor-supplied protocol. Briefly, the chosen target sequence was amplified, after which the dsDNA amplicon was purified by ethanol precipitation. The digestion was then performed in a 50 µl mixture by combining 34 µl water, 5 µl 1X NEBuffer4 (New England Biolabs, MA, USA), 10 µl amplified DNA and 1µl CaC8I. After overnight digestion, the DNA was again purified by ethanol precipitation, and then suspended in a Tris (pH 7.6) buffer, the same as the undigested control sample. For testing, multiple ratios of the digested and undigested DNA were combined.

2.2.1.3 *qPCR*

The crossing point (Cp) of a qPCR amplification curve refers to the cycle number where the fluorescence exceeds a given threshold, thus indicating the presence of a PCR product in a sufficient amount to be detected. The crossing point is related to the

amplification efficiency (η_{PCR}) and the initial template concentration (X_0). Changes in the crossing point (ΔC_p) and percent changes in the initial template concentration (ΔX_0) can be correlated as shown in Eq. 2.1:

$$\Delta X_0 = (1+\eta_{PCR})^{\Delta Cp} \text{ X } 100\%. \qquad \textbf{Eq. 2.1}$$

The amount of the initial template was the same for all the samples used in this study. However, an increasingly damaged template was expected to cause a decrease in the amplifiable DNA, thereby producing a shift in the qPCR crossing point. The magnitude of this shift was used to infer the extent of DNA damage.

2.2.1.4 *HRMA*

For HRMA, DNA melting curves were analyzed in the LS32 either immediately after PCR (without the need to take the samples out of the LS32) or after UV damage. The same sample volumes (10 µl) and capillaries were used for HRMA as for the qPCR. The melting of all samples was performed by heating each sample from 50° to 95° C, at a heating rate of 0.3° C/s. The melt curves were analyzed on the native BioFire software, and also parameterized using a numerical software (MATLAB, MathWorks, MA), echoing the technique demonstrated by another group [94].

2.2.1.5 *Gel Electrophoresis*

When gel electrophoresis was used for size or quantity evaluation, 8 µl of each sample (plus 2 µl loading dye) was loaded in a 2% agarose gel (Sigma, USA), immersed in a TBE buffer, and 110 V was applied for 45 minutes (Galileo Bioscience, MA, USA; Enduro power supplies, Labnet International, Inc., NJ, USA). The DNA ladder N3234S (New England Biolabs, MA, USA) was used as a sizing reference. After electrophoresis,

the gels were imaged using a UV transilluminator (GelDoc-It, UVP LLC, CA, USA). We performed subsequent excision of the products manually.

2.2.2 Experimental Design

2.2.2.1 *qPCR to Detect CPDs*

To detect intramolecular DNA damage (CPDs) using qPCR, two different primer sets shown in Table 2-1 were used, targeting a 112-bp (base pair) and a 106-bp segment of the pET-24b plasmid (Novagen, Darmstadt, Germany).

Table 2-1: Primer sets and associated details for DNA damage studies.

Experiment Set	**Primer sets and amplified regions**	**Product size**	**Primer T_m**
qPCR to detect CPDs, qPCR and HRMA to detect CPDs in multiplex PCR	Source: E.coli Low risk sequence: Amplified region on plasmid: 3442-3553 Forward: 5'- AGT TCG GTG TAG GTC GTT CG-3' Reverse: 5'- GTC TTA CCG GGT TGG ACT CA-3' High risk sequence: Amplified region on plasmid: 4495-4600 Forward: 5'- ATT CTC ACC GGA TTC AGT CG-3' Reverse: 5'- GAT TCC GAC TCG TCC AAC AT-3'	112-bp 106-bp	56.8° C 56.5° C 54.5° C 54.7° C
HRMA to detect CPDs	Source: E.coli Strain: HF 4704 Amplified region on plasmid (ΦX174-1): 260-369 Forward: 5'- GGT TCG TCA AGG ACT GGT TT -3' Reverse: 5'- TTG AAC AGC ATC GGA CTC AG-3'	110-bp	55.1° C 54.9° C
HRMA to detect DSBs	Source: E.coli Strain: HF 4704		

	Amplified region on plasmid (ΦX174-2): 802-916 Forward: 5'- CAG AAG AAA ACG TGC GTC AA-3' Reverse: 5'- GCC TTT AGT ACC TCG CAA CG-3'	115-bp	53.7° C 55.9° C

The two PCR targets were selected such that one would be more susceptible to UV damage than the other. Others have done this by amplifying targets of significantly different sizes [81]. However, a goal of this present work was to use PCR targets below 200-bp, thereby enabling rapid PCR thermocycling [96]. Therefore, the entire plasmid sequence was analyzed with MATLAB to identify regions of high and low damage susceptibility, based on the presence of specific base pairs (TT>TC>CT>CC) and their complements. Risk of damage for the respective based pairs was correlated to the damage site frequency values previously obtained by Douki and Cadet for UV-C [97]. The potential damage sites and their relative degree of damage risk are shown in Figure 2-1. The high risk 106-bp sequence is approximately 50% more susceptible to UV damage than the low risk (112-bp) sequence. qPCR was used to evaluate UV damage of both plasmid regions under identical exposure conditions. The resulting shift in qPCR crossing point was correlated to the template exposure time for the "high risk" and the "low risk" targets.

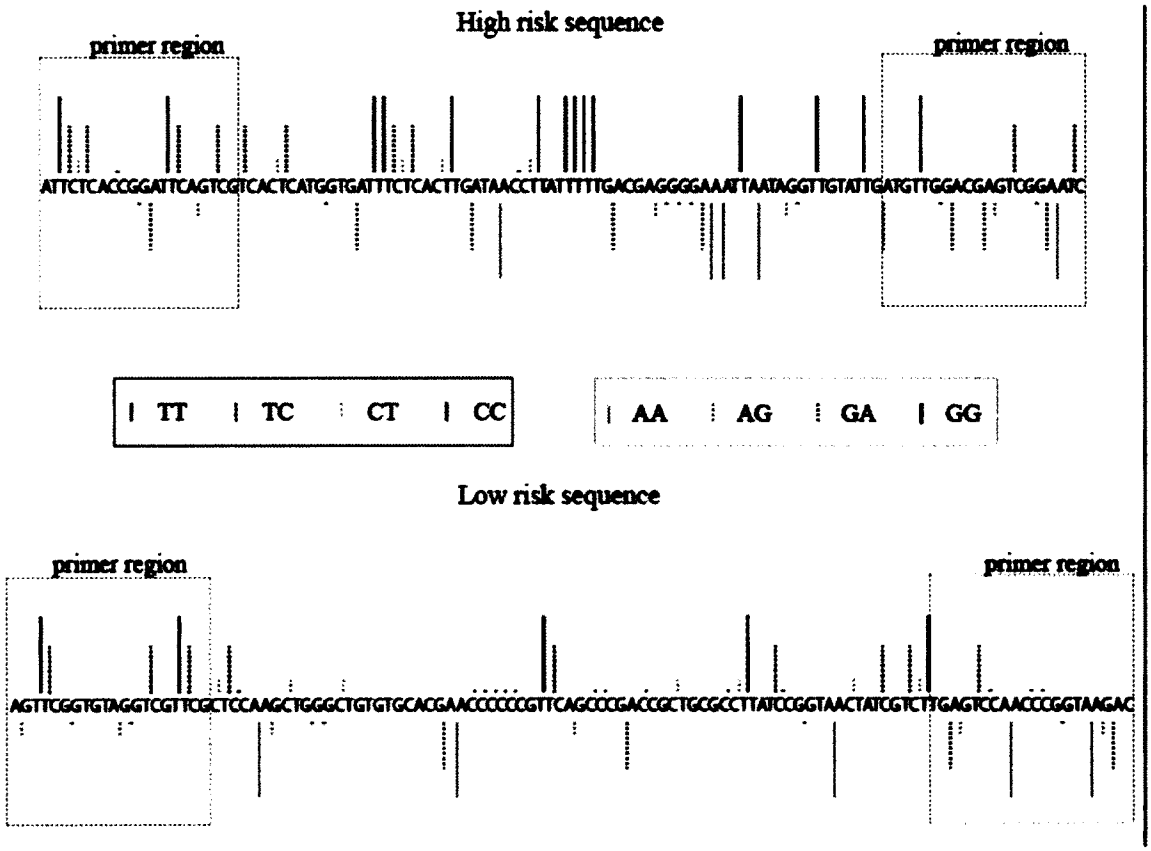

Figure 2-1: The high risk and low risk DNA sequences, with vertical lines indicating the location and relative susceptibility of the potential dimerization sites. Using the risk scale developed by Douki and Cadet, the high risk sequence is about 50% more susceptible to UV damage than the low risk sequence.

For these experiments, the template DNA samples were loaded into the glass capillaries. The control (undamaged) samples were left in the refrigerator and the rest of the samples exposed to UV-C radiation ranging from a few seconds to several minutes. After exposure, the PCR reagents were added, reducing the template concentration from 136 pg/μl to 13.6 pg/μl. The samples were subsequently amplified in the LS32 instrument for 30 cycles at temperatures of 96° C – denaturing, 62° C – annealing, and 72° C – extension. The damage in the DNA samples was observed by comparing the crossing points (Cp) of their amplification curves with those of non-irradiated samples.

2.2.2.2 *HRMA to Detect CPDs*

HRMA was used to detect damage (CPDs) to PCR-amplified DNA samples. A PCR mixture was used with forward and reverse primers shown in Table 2-1 targeting a 110-bp (base pair) segment of the ΦX174 bacteriophage (New England Biolabs, MA, USA), ΦX174-1. For these tests, aliquots from a bulk PCR mixture were used. The PCR protocol for amplification in the LS32 consisted of 40 cycles, with temperatures of 96° C – denaturing, 65° C – annealing, and 72° C – extension. At the conclusion of the PCR, HRMA was performed on all samples. The capillaries were then placed inside the UV crosslinker. The crosslinker was turned on and one capillary was removed every 10 seconds so that the last capillary removed had experienced a total of 10 minutes of radiation exposure, resulting in a total of 61 samples. The capillaries were then returned to the LS32 instrument for a subsequent HRMA. The results from HRMA were also compared with the gel electrophoresis.

HRMA was also used to analyze its ability in detecting the damage to PCR-amplified DNA when exposed to UV-A, UV-B and UV-C radiation. The targeted 110-bp segment of the ΦX174 DNA as given in Table 2-1 was amplified using 40 cycles, with temperatures of 96° C – denaturing, 65° C – annealing, and 72° C – extension. At the conclusion of the PCR, HRMA was performed on all samples. Being a closed tube technique, the amplicon inside each of the capillaries was subsequently exposed to UV-A, UV-B and UV-C radiation. The UV crosslinker was used with interchanging UV-light bulbs for each of the UV-A, UV-B and UV-C exposures. The capillaries were split into three groups of five samples each. We exposed each of the five samples to different amounts of UV exposure times with each type of UV exposure. A subsequent HRMA

was performed on all the exposed PCR-amplified samples in comparison with the unexposed PCR-amplified samples.

2.2.2.3 *HRMA to Detect DSBs*

DSBs were created using a restriction enzyme and HRMA was used to quantify any resulting differences in the DNA melting behavior. The approach was to amplify a 115-bp long segment of the ΦX174 bacteriophage initially, ΦX174-2 with primers given in Table 2-1, and using a 40-cycle PCR with amplification temperatures of 96° C – denaturing, 65° C – annealing, and 72° C – extension. CaC8I was used for these tests because this endonuclease generates blunt cleavages. Therefore, the amplicon would only be divided into separate pieces, such that the complementary pairing of all bases (hydrogen bonding) would be identical to that of the undigested DNA. Furthermore, this enzyme would cleave the amplicon into significantly different strand lengths (39-bp and 76-bp), making them individually distinguishable using gel electrophoresis. The undigested DNA was mixed with the digested DNA in varying proportions and loaded with 1 X of the LCGreen Plus dye into the glass capillaries for HRMA on the LS32. Afterward, the samples were also analyzed using gel electrophoresis.

2.2.2.4 *qPCR and HRMA to Detect CPDs in Multiplex PCR*

Multiplex PCR has been performed by adding two different primer sets in the PCR mixture thereby amplifying two different regions, namely low risk sequence and high risk sequence (see Table 2-1) in the ΦX174 DNA. The PCR protocol consisted of 30 cycles, with temperatures of 96° C – denaturing, 62° C – annealing, and 72° C – extension. The amplification protocol had to be optimized in order to amplify the two targets in a single capillary. The PCR mixture was loaded into glass capillaries and each

of the capillaries was exposed to UV-C radiation in the UV-crosslinker for different exposure times. The exposed capillaries along with the unexposed control sample were amplified and analyzed using the LS32.

2.3 Results and Discussion

2.3.1 qPCR to Detect CPDs

qPCR was used to detect DNA damaged from UV irradiation prior to amplification. The crossing points were obtained from the individual amplification curves generated on the LS32. The crossing point for each damaged sample was compared against the average crossing point of the undamaged samples. The change in crossing point as a function of exposure time is shown in Figure 2-2.

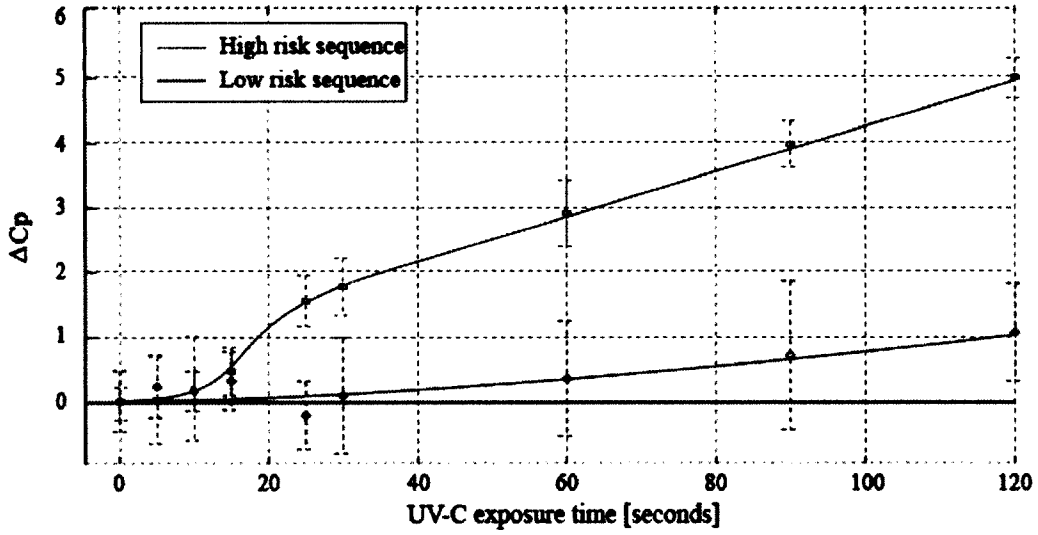

Figure 2-2: The low risk DNA sequence shows a remarkably slower degradation than the high risk sequence. The lower exposure times 5, 10 and 15 seconds have data points from 16 samples each (n = 16). The higher exposure times 25, 30, 60, 90, and 120 seconds have data points from 8 samples each (n = 8). The exposure time was plotted against the difference in the cycle number averaged from multiple samples at each of the exposure times.

These results clearly indicate that the two amplified DNA sequences have a distinctly different sensitivity to UV-C radiation. With high sample numbers per batch (n = 16 in this instance), the difference in damage sensitivity was detected after as little as 15 s of irradiation. According to the relative damage risks of the two DNA targets (see Table 2-1), only a 50% difference in damage was anticipated. Interestingly, however, the effect appeared to be much more significant. This could be caused in part by the high risk sequence being more susceptible to damage due to the clustered nature of the damage sites. However, it is beyond the scope of this work to explore the compounding damage mechanisms that are implied in this data set. Rather, the emphasis of this section is to highlight the ability of qPCR as an analytical tool for such investigations.

While qPCR proved very adept at detecting template damage prior to PCR, HRMA did not. After qPCR, the samples were further examined by HRMA, as well as by gel electrophoresis. The DNA melting curves and the gel electrophoretograms revealed no statistical difference between the irradiated and control samples. The DNA concentration of all amplified samples was approximately the same, since each qPCR was continued into the plateau phase. The lack of shape change in the melt curves (shown in Figure 2-3) provided a strong indication that no damaged DNA could amplify, or at least that no UV-C damage was propagated into the PCR product (as a base substitution or partial mismatch, for example). Whichever the case, there was clearly no record of the radiation exposure in the PCR amplicon. In contrast, the high accuracy, precision, and ability to quantify the amplification products of nucleic acids in real time make qPCR a preferred method for DNA analysis.

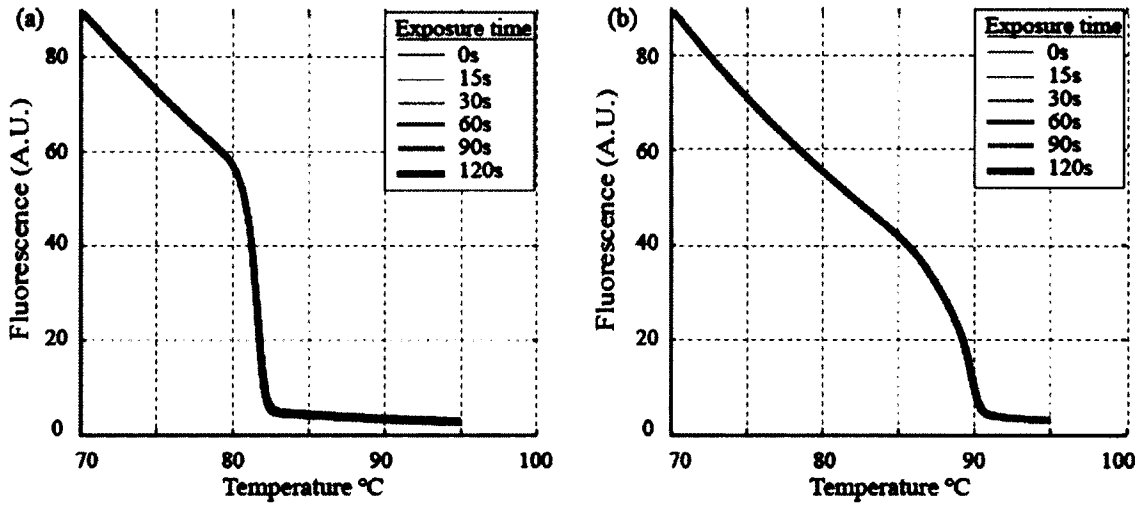

Figure 2-3: DNA melting curves for PCR amplicon of the: (a) "high risk" sequence, and (b) "low risk" sequence, for six different UV-C exposure times. All six data curves exactly overlap. This lack of shape change is an indication that the PCR product is identical in sequence and structure to the healthy DNA.

2.3.2 HRMA to Detect CPDs

When ΦX174-1 DNA was irradiated after PCR, the melting curves were observed to change as a function of UV-C exposure time. The derivative plots of the fluorescence curves are shown in Figure 2-4-a. The Tm of the undamaged PCR product was approximately 81.5° C. The derivative curve was found to peak (which occurs at the Tm) at lower temperatures (see Figure 2-4-b) and reach a lower maximum (see Figure 2-4-c) with increasing UV exposure. This was attributed to intramolecular changes in the DNA (CPDs in this instance), which altered the overall hydrogen bond energy and hence the melting behavior.

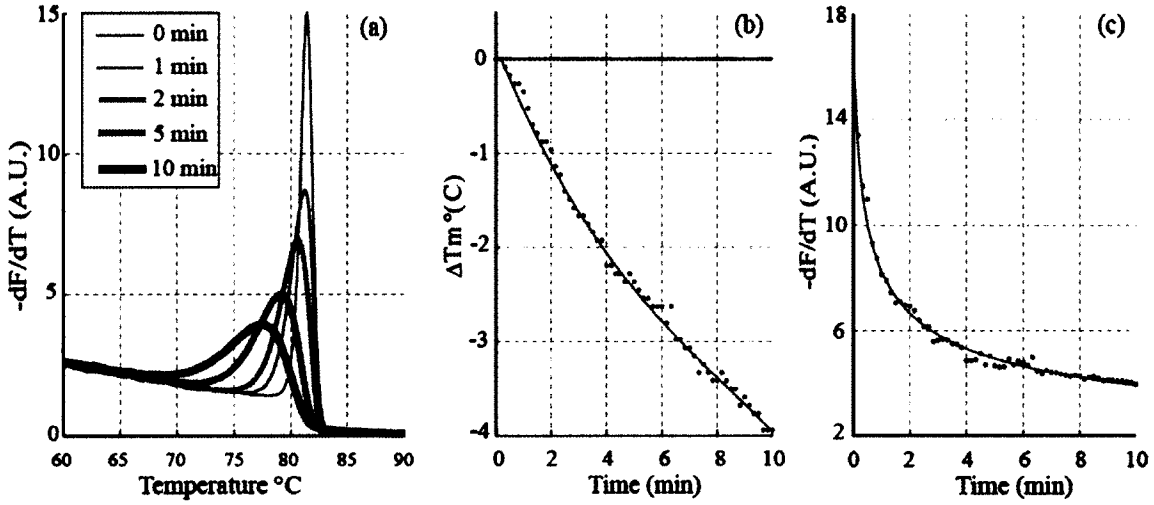

Figure 2-4: The derivatives of the fluorescence versus temperature plots obtained by high resolution melting analysis (HRMA) reveal changes in the melting behavior due to the formation of CPDs. The curves of ΦX174-1 in (a) are the derivative plots for 5 samples irradiated from 0 seconds to 10 minutes in a UV-C crosslinker. The plot in (b) shows how the Tm changes with exposure. The plot in (c) shows how the peak height changes with exposure. The plots in both (b) and (c) consist of 61 data points obtained from samples irradiated in 10 second increments between 0 and 10 minutes.

To verify that the shifting in the melting curves was not caused by double-strand breaks, samples were also evaluated using gel electrophoresis. As seen in Figure 2-5, no band broadening or multiple bands were observed. Only a slight decrease in maximum intensity was revealed, likely due to the decreased number of undamaged base pairs available for ethidium bromide intercalation. The consistency of the electrophoretic mobility of the DNA indicated that the molecular mass of the DNA remained unchanged; no double-strand breaks were present.

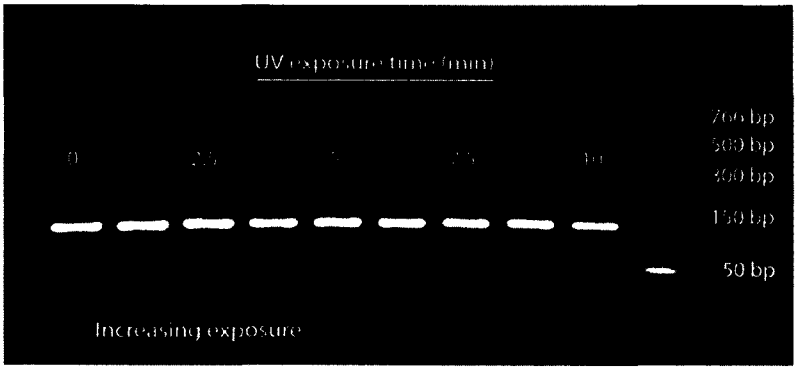

Figure 2-5: ΦX174-1 samples were analyzed by gel electrophoresis after HRMA. The lack of multiple bands or band broadening indicated that no fragmenting of the DNA occurred during the UV exposure. Other than that, though, little details of the damage itself can be obtained from such electrophoretograms.

Unlike such analytical methods that differentiate by size and/or mechanical mobility, HRMA – as a measure of binding energy – precisely reveals the intramolecular changes to the DNA molecule. In addition, being essentially a closed-tube process, HRMA may provide a welcome analytical simplicity to studies with which this approach is compatible.

Figure 2-6 demonstrates the differences in DNA damage with respect to the exposure type of UV radiation. In the results presented in Figure 2-6, the UV-induced direct base damage can be observed in the UV-B and UV-C exposed samples over time, but not the UV-A sample. This supports the findings of other researchers who have reported that UV-B and UV-C can cause damage to DNA by direct absorption of radiation by the bases and UV-A causes damage to DNA by photosensitization followed by oxidative damage (indirect damage) [1]. Since these present experiments were performed with plasmid DNA (PCR-amplified) rather than with living cells, UV-A did not generate base damage.

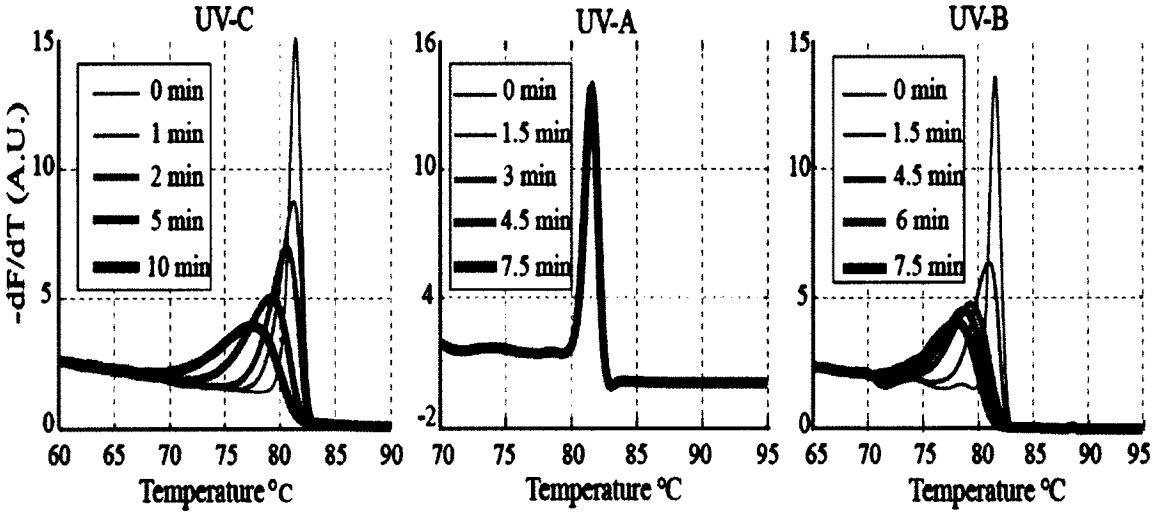

Figure 2-6: PCR-amplified samples exposed to different types of UV-radiation.

2.3.3 HRMA to Detect DSBs

HRMA was evaluated to determine its ability to detect double-strand breaks. Figure 2-7-a shows the derivative plots of ΦX174-2 with the undigested DNA, the completely digested DNA, and four different combinations of the undigested and digested DNA mixtures. In Figure 2-7-b, the individual melt curves of each of the combinations were plotted.

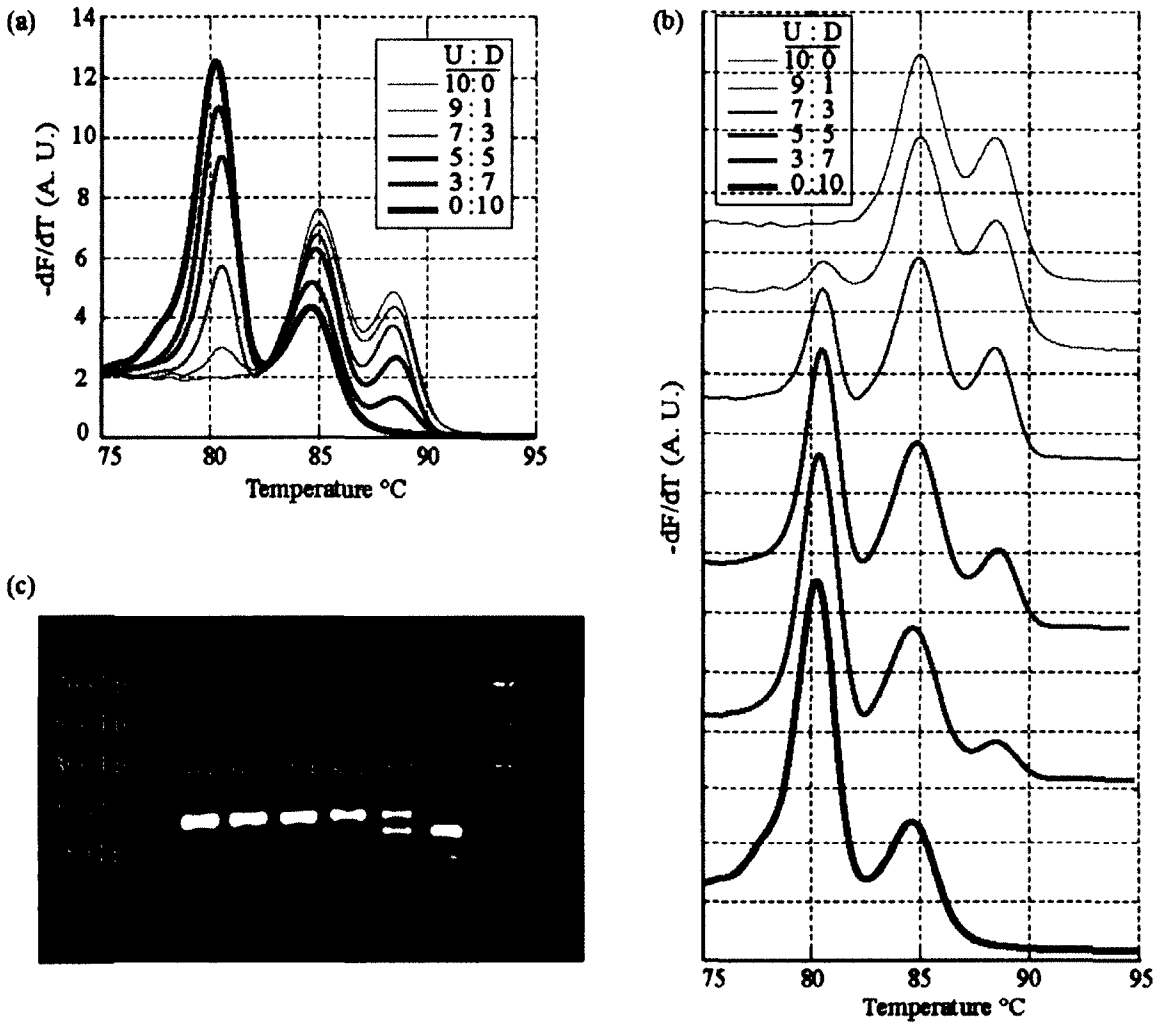

Figure 2-7: Detection of strand breaks in the ΦX174-2 sequence. (a) Melting analysis clearly identifies the degradation in the samples in the form of double-strand breaks. The legend denotes the ratio of undigested (U) to digested (D) DNA in each sample. As a single-strand (115-bp, GC% = 50.4), the DNA exhibits a two-regime melting profile (Tm ≈ 85°/88°). When the amplicon was cleaved into two strands, the longer fragment (76-bp, GC% = 42.1) melts at nearly 80.5°, and the shorter fragment (39-bp, GC% = 66.7) melts near 84.5°. (b) The individual melt curves of each of the U:D combinations showing the formation of strand breaks. (c) The gel electrophoresis of these samples confirms the size of the DNA fragments and the completeness of the digestion.

The derivative plots (Figure 2-7-a and Figure 2-7-b) of the undigested DNA (see U:D of 10:0 in the legend) reveal two peaks, indicating that the DNA has a two-regime

melting profile. The peaks are at approximately 85° and 88° C. Since the nucleotides guanine and cytosine have a higher binding energy than does the adenine/thymine pairing, local DNA sequence significantly affects melting behavior. In the 115-bp segment evaluated here, the total percentage of hydrogen bonds that were G/C nucleotide pairs (called GC%) was 50.4%. However, distribution of the G/C pairs was concentrated to a particular region of the DNA. This caused a bimodal melting behavior. The two-regime melting curve was confirmed to be from a single 115-bp product using gel electrophoresis (see Figure 2-7-c). The derivative plot of the completely digested DNA (U:D of 0:10) again shows two melting peaks, around 80.5° and 84.5° C.

However, the digested sample was essentially a heterogeneous mixture of the two digestion fragments (76-bp, 39-bp). This was confirmed by gel electrophoresis (see Figure 2-7-c). The individual bands were excised, re-purified and subsequently analyzed by HRMA. The melts of the individual digestion fragments (data not shown) confirmed that the 80.5° C peak was from the 76-bp fragment and the 84.5° C was the melting of the 39-bp fragment. This counter-intuitive result (the smaller fragment melting at the higher temperature) is due to the fact that HRMA is particularly sensitive to GC%, and that the longer fragment had a significantly lower GC% (42.1%) than the shorter fragment (66.7%).

The samples containing a mixture of digested and undigested DNA had melt profiles that include all four melting peaks (85° and 88° from the undigested, 80.5° and 84.5° from the digested DNA). Three peaks are only visible in the melt curves, though, since the 84.5° and the 85° peaks are almost exactly superimposed. Since the 80.5° peak is completely absent from the undigested melt curve, any melting at this temperature is a

clear indicator of DNA fragmentation. Even a melt of the 10% digested sample definitively reveals the presence of the fragmented DNA. In contrast, the gel electrophoretogram of the same sample (9:1) does not show the digested portion. Even the sample that is 30% digested (7:3) displays the fragments only faintly.

Clearly, HRMA is a much more sensitive tool than gel electrophoresis for detecting a low concentration of fragmented DNA. Sensitivity in this context refers to the lower threshold of sample damage that can be clearly detected using a given analytical method. For HRMA, the 10% damaged sample produced a measurable change (Figure 2-7-a), whereas with the gel electrophoresis, the 50% damaged sample was the first that revealed a noticeable second band (Figure 2-7-c).

The temperature curves from Figure 2-8 were extracted from the peak height data points from HRMA of the ΦX174-2 sequence. The ascent in the curve 80.5° C identifies the gradual formation of the 76-bp fragment with an increase in the ratio of the digested DNA in the mixture with a simultaneous descent in the curves 84.5° C and 88° C. The curve 88° C nears zero in the 0:10 mixture ratio denoting the diminishing of the 115-bp fragment. The decrease in the curve 84.5° C is in accordance with the formation of the 39-bp fragment from the 115-bp fragment.

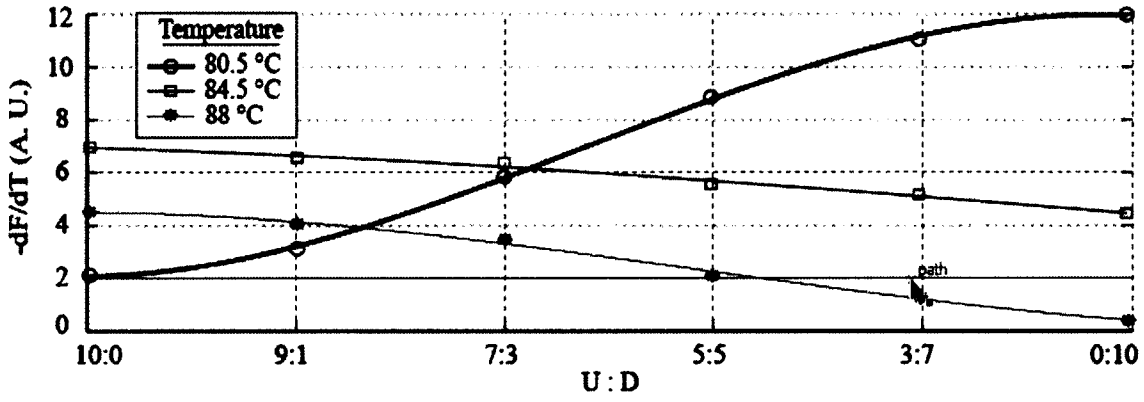

Figure 2-8: The gradual change in the peak height at different temperatures with increase in the digested DNA in the mixture denotes the presence of the double-strand breaks in the ΦX174-2 sequence.

This work demonstrates that HRMA is very effective at detecting DSBs. While CPDs cause changes in the hydrogen bonding between the two strands of the dsDNA, there is no change in the nucleotide pairing with DSBs; all bases are still healthy and all remain bonded with their complement. Rather, the strands are just divided into shorter fragments. It is known that the thermal stability of dsDNA is partially enhanced by the nearest-neighbor construct of the DNA sequence [98, 99]. Therefore, longer fragments melt at higher temperatures than do shorter fragments having the same GC%. As shown in this work, the resulting changes in the HRMA curves for even slightly fragmented DNA can be significant. This approach can be applied to all mechanisms of DNA fragmentation, whether through enzymatic digestion (as done here), chemical damage, ionizing radiation, or other causes.

Since HRMA is a non-destructive technique, gel electrophoresis of the samples can be performed afterward. However, there is a significant advantage to using HRMA instead of gel electrophoresis. For example, HRMA in small batches is much faster. For these HRMA experiments, each sample was analyzed in 2.5 minutes. In contrast, the gel

analysis needed 60 minutes for each run. There are also many processing steps such as the gel preparation, sample preparation/loading, and manual evaluation of the gel samples with a UV transilluminator, which can be avoided with HRMA. In addition, HRMA requires no additional instrumentation, since the thermocycler used for this work (LS32) possesses both PCR and HRMA functionality. Since HRMA is also much more sensitive to DSBs (see Figure 2-7), further damage studies would be well suited to this analytical methodology.

2.3.4 qPCR and HRMA to Detect CPDs in Multiplex PCR

qPCR was used to detect differences between the DNA samples that experienced varying degrees of radiation exposure. HRMA was used to distinguish the susceptibility of DNA to UV damage between two different targets in the template (the high risk target being more susceptible to UV damage compared to the low risk target). The two sequences targeted by the two different primer sets mixed together in the PCR mixture (multiplex PCR) are given in Figure 2-1. The amplification curves of the multiplexed samples after being exposed to UV-C radiation for 0, 10, 20, 40, 60, and 100 seconds obtained from LS32 are shown in Figure 2-9.

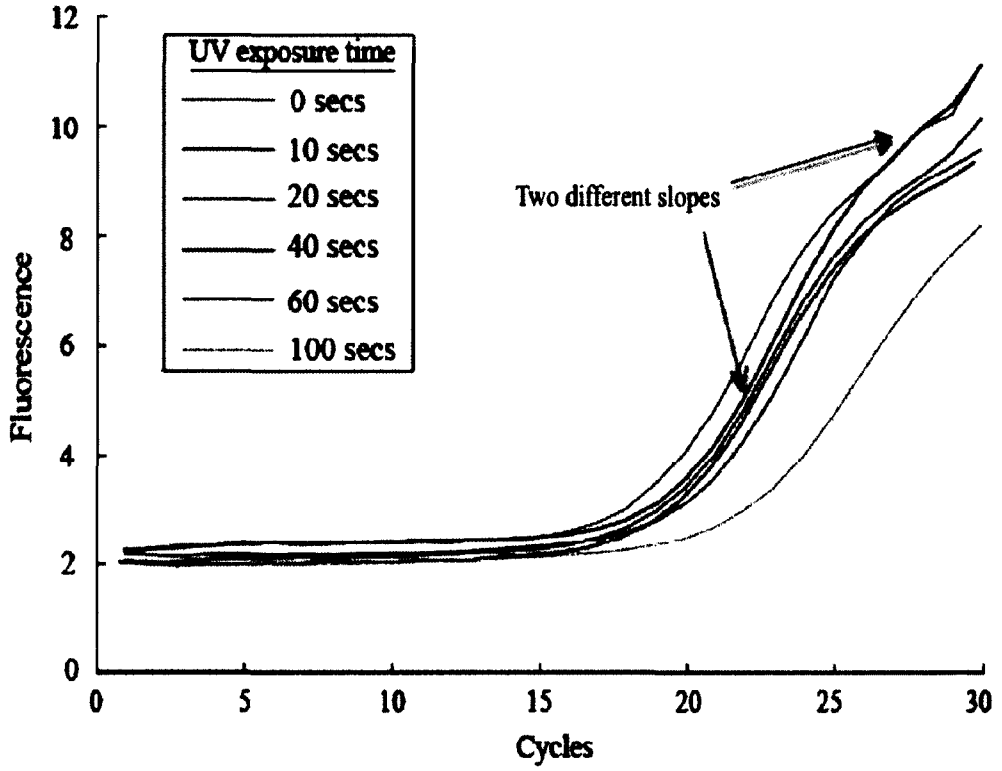

Figure 2-9: Amplification curves of multiplex PCR exposed to UV-C radiation obtained from LS32.

The amplification curve of the control sample (0 seconds exposed) clearly depicts the two different slopes that correspond to the two different sequences being amplified. The gradual delay observed in the crossing points (the cycle number showing the start of rise in the amplification curve from its baseline) with an increase in the exposure time can be seen from Figure 2-9. The qPCR data obtained in about 15 minutes proves that it can be a proficient technique in the early detection of DNA damage.

Subsequent to qPCR, the samples were analyzed using HRMA in the LS32 without the need of additional processing steps/instrumentation. The derivative peaks of the different exposed and amplified multiplexed samples are given in Figure 2-10.

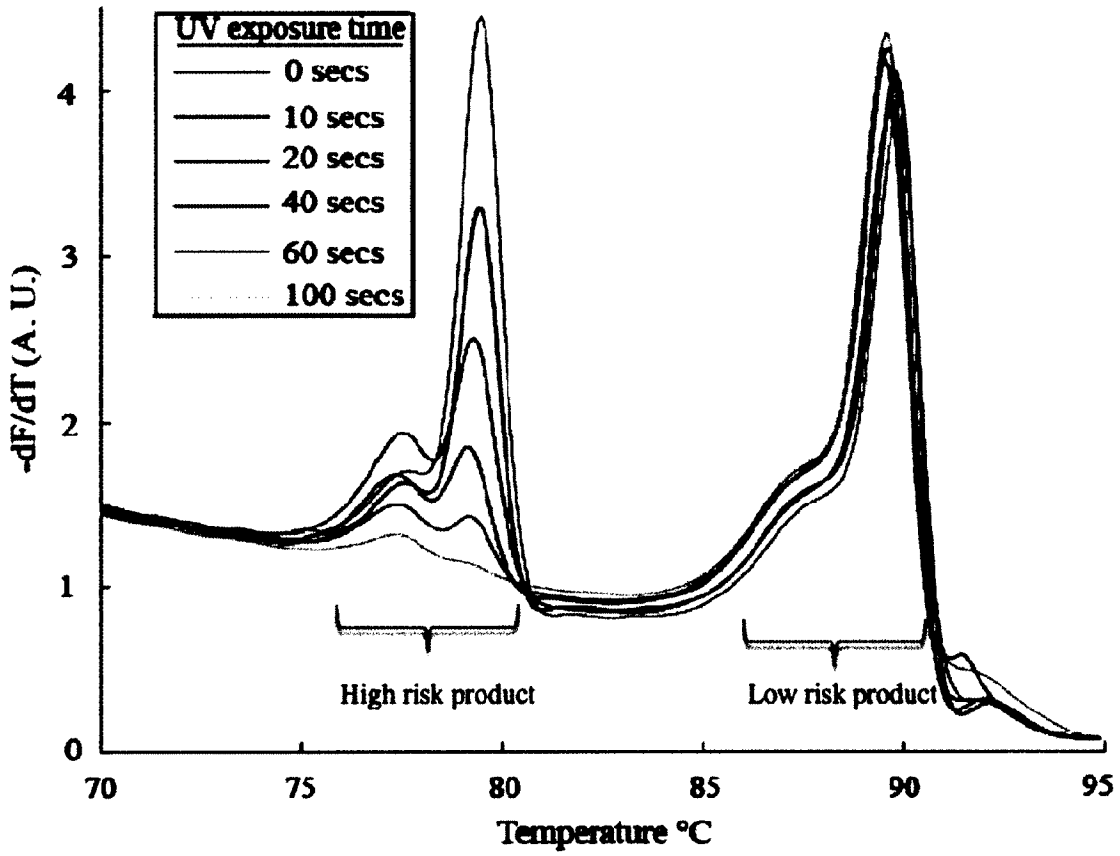

Figure 2-10: The derivative curves of the different UV-C exposed and then amplified multiplexed samples.

The high and the low risk sequences are clearly identified by the HRMA. The melting temperature of the high risk sequence is at ~80° C and of the low risk at ~88° C. The gradual peak height decrease in the high risk sequence with an increase in the exposure time can be observed from the derivative curves of Figure 2-10. This gradual decrease of the peak height in the high risk sequence corresponds to the increase in the DNA damage (formation of CPDs). The differences in the peak height of the melt curves around the high risk melting temperature is also because the amplification is stopped at 30 cycles which did not allow all the samples to reach their plateau phase in the amplification curve. Due to the damage in the samples in accordance with the exposure

time, the more exposed samples had lesser time to amplify before the amplification is stopped, which provided facilitated damage detection in the high risk sequence using HRMA. In the case of the low risk sequence, there was no sign of any damage corresponding to the exposure times. This implies that all the low risk samples had already reached the plateau phase in their amplification that made it difficult to detect any damage in the low risk sequence using HRMA. In summary, HRMA is able to detect damage in DNA prior to PCR, provided the amplification is stopped before the DNA reaches its plateau (maximum final concentration), which might not be feasible in most of the applications. For this reason, qPCR rather than HRMA would be preferred as an efficient technique for the detection of damage (CPDs) occurring in pre-amplified DNA.

2.4 Conclusions

The results of this chapter indicate that qPCR and HRMA can be effective tools in the study of DNA damage. This includes intramolecular damage as well as strand breaks. In this work, CPDs were created by exposing samples to UV radiation either before or after DNA amplification. When exposed before amplification, the initial concentration of amplifiable DNA decreased. This decrease was revealed by a distinct shift in the qPCR crossing point. By examining different regions of the DNA genome in this way, the relative susceptibility of each to UV damage was evaluated. This suggests that qPCR could be a reliable and efficient technique for the quantification of many types of intramolecular DNA damage, on both the global (genome) and local (gene) level. When samples were exposed to UV radiation after amplification, the generated CPDs were found to alter the hydrogen bonding energy within the damaged dsDNA molecules. This produced a decrease in the thermal stability of samples, which was detected using

HRMA. Significantly, this analysis method is a closed tube technique, needing no purification. Moreover, it is a single step process that can be carried out on existing real-time PCR instrumentation. In other experiments, DSBs were induced using restriction enzyme digestion. Fragmentation of DNA molecules was shown to reduce their thermal stability. DNA samples with even a small amount of DSBs exhibited a melting behavior distinctly different from that of undamaged samples. These differences were easily detected using HRMA. The results of this work indicate that HRMA is both faster and more sensitive than gel electrophoresis.

The results of this chapter confirm that qPCR and HRMA can be used to evaluate the two damage mechanisms (UV-C and CaC8I) experimentally tested. Furthermore, the damage characteristics (CPDs and DSBs) are common products of many harmful environments (e.g. high-energy radiation, chemical exposure, etc.). Therefore, the underlying physical manifestations that are measured by the techniques used in this article (amplifiability for qPCR, and thermal stability for HRMA) may be generally applicable. Main advantages of these methods include procedural simplicity and sensitivity. There is a great need for such technologies in the advancing research areas of radiation biology. In particular, the virtually real-time nature of these techniques can have a significant impact in the study of DNA repair kinetics. The ability to quantify the DNA damage through the presented techniques, qPCR and HRMA can also be applicable in various areas of biotechnology such as biosafety, genotyping, and genetic stability testing.

CHAPTER 3

EXPERIMENTS ON AN INTEGRATED MICROFLUIDIC SYSTEM

3.1 Background

The fabrication of microfluidic devices is a complex series of processes, each of which needs to be optimized for desired performance. The choice of the substrate material greatly determines the fabrication methods that are required. Glass and silicon are the most commonly used substrates for microfluidic devices. The superior qualities of glass such as high chemical and heat resistance, insulating properties, and low optical absorption offer a wide range of applications in bio-MEMS, RF-MEMS, optical MEMS, and chemical and biomedical devices [100-102]. In the presented work, we have chosen glass as the substrate for our microfluidic device. For glass microfluidics, the fabrication process flow must be performed in a cleanroom environment, and generally includes: photolithography, glass patterning, and bonding. This chapter discusses the details of microfabrication including photolithography, etching and bonding that are used to form the glass microdevice. The complete microfluidic system set up for on-chip PCR is discussed and the results are presented.

3.1.1 Photolithography

Photolithography, also called UV lithography, is the process of transferring patterns from a photo mask onto a substrate. The major steps in photolithography include

substrate cleaning, applying photoresist to the substrate, mask alignment, exposure and development.

The initial step in photolithography is to clean the substrate and apply a layer of required photoresist on top of the substrate using a spin coater. The spin coater uses a centrifugal force to coat the substrate with photoresist evenly. Two types of photoresist are used in lithography namely, positive and negative. A positive photoresist is used to transfer the pattern as it is from the mask onto the substrate, whereas a negative photoresist is used to transfer the pattern opposite to that on the mask. Following the application of the photoresist, the substrate is exposed under the mask to UV light in a mask aligner. In the case of the positive photoresist, the UV exposure interacts with the photoresist chemically, thus making it weaker in the areas exposed. The interaction of the UV light with the negative photoresist polymerizes it, making it stronger in the areas exposed. The substrate is then immersed in a developer solution, which dissolves the weaker parts of the photoresist (the exposed areas in the case of positive photoresist and the unexposed areas in the case of negative photoresist). The micropattern is now transferred from the mask onto the substrate, which completes the initial stage of fabrication.

3.1.2 Glass Patterning

Glass patterning for microfluidic devices can be done using two different approaches, namely wet and dry etching processes. Wet etching is an isotropic etch causing glass etching in both vertical and horizontal directions. Wet etching is performed in a hydrofluoric acid (HF) based solution. Dry etching process results in an anisotropic etch profile caused due to its directionality. Dry etching is usually performed in a plasma

induced reaction ion etch (RIE) chamber. A variety of etchants are used depending on the glass composition and the etch depths required for the application. Table 3-1 gives a summary of different etching parameters used for glass.

Table 3-1: Typical glass etching parameters [57].

Etch process	Etchants	Masking layers	Etch rate
Wet etching	HF/HCl (10/1) HF HF/NH_4F	▪ Chrome/gold/photoresist ▪ Amorphous silicon ▪ Molybdenum/photoresist ▪ Amorphous silicon/amorphous silicon carbide/photoresist	Up to 7-8 μm/min (for Corning 7740 glass)
Dry etching	SF_6, C_4F_8, CF_4, CHF_3	▪ Nickel plated ▪ Thick amorphous silicon ▪ SU8 resist	Up to 0.5-0.8 μm/min

Dry etching of glass is only chosen when anisotropic profiles are required and etch depth is not much of a concern. Dry etching of glass is a relatively slow process requiring a low pressure ranging from 5-10 mTorr and producing an etch rate of 0.5-0.7 μm/min (as opposed to 7-8 μm/min for Corning 7740 glass through wet etching). With the thermal conductivity of glass being 100 times lower than that of silicon, the dry etching process (using plasma RIE reactors) creates temperature gradients across the substrate [57]. The gradients can lead to damage to the substrate and also result in poor selectivity relative to the mask. Gases used for dry etching of glass include SF_6, C_4F_8, CF_4, and CHF_3 [103-106]. The low selectivity necessitates thick masking such as electroplated Ni, amorphous silicon, SU-8, and bulk silicon [57, 104, 107]. The requirement of etch depth in the microchannels of around 70-80 μm with a minimal

roughness made us choose wet etching rather than dry etching of glass for the microfluidic system.

3.1.3 Glass-to-glass Bonding

The glass bonding techniques that are used for microfluidic applications can be categorized mainly into direct/fusion, anodic and adhesive bonding. The type of bonding is chosen according to factors like the device application, the surface characteristics of the materials to be bonded or any temperature limitations. A brief summary of the different bonding techniques is given in Table 3-2.

Table 3-2: Major glass bonding techniques.

Bonding technique	**Substrate material**	**Typical parameters**
Direct/fusion bonding [57, 102, 108, 109]	Glass/glass	Around 600° C
	Sequential plasma activation of glass/glass or silicon/glass	O_2 followed by N_2 plasma, 115-400° C
Anodic bonding [57, 109-111]	Glass/silicon or Glass/silicon/glass	300-550° C, up to 1kV
Adhesive bonding [57, 109]	Glass/glass or glass/silicon	Around 150° C

Fusion bonding is performed in annealing furnaces and requiring high temperatures. The use of really high temperatures may cause fractures due to substantial temperature gradients in the substrate. For most types of glass substrates, the softening point being around 600° C might cause distortions in the channels [57]. Direct bonding requires clean bonding surfaces either by rigorous cleaning or by using plasma activation of surfaces. Surface activation followed by lower annealing temperatures has been

reported to increase bond strengths between the substrates [112, 113]. Anodic bonding is used typically for bonding silicon to glass provided the chosen glass substrate has a thermal expansion coefficient matching with the silicon. Glass/glass anodic bonding is also achieved using metallic intermediate layers [57, 114]. Adhesive bonding is a simple and less inexpensive technique using polymers, usually thermoplastic materials. Various groups investigated the use of adhesives such as parylene, SU-8, and polyimide [115-117]. The major disadvantage in the use of adhesive layers is the possibility of the adhesive layers to get into the microchannels. Taking into consideration all the available bonding techniques, we have chosen to activate the glass surface, apply pressure, and then anneal it at low temperatures when compared to the other available techniques.

3.2 Experimental Materials and Methods

3.2.1 Types of Substrates Used

Glass is composed of several different oxides, which affect the etching behavior and also the etchants used. The oxides contained in glass like CaO, MgO and Al_2O_3 create insoluble products when they react with the HF solution, thereby decreasing the etch rate and increasing the surface roughness [57, 101, 107]. So it is essential that the glass chosen for fabrication should have less proportions of the insoluble oxides, thus forming smoother microchannels. We were able to create microfluidic patterns on two types of glasses, namely the borosilicate (also called pyrex/corning) and the soda lime glass. Soda lime glass has been purchased from Fisherfinest and the borosilicate glass (more specifically, Borofloat 33) from Bullen. The compositions of both glasses are given in Table 3-3 as per the manufacturers.

Table 3-3: Composition of the glasses used.

Components	Borosilicate glass	Soda lime glass
SiO_2	81%	72.20%
B_2O_3	13%	
Na_2O	4%	14.30%
Al_2O_3	2%	1.20%
CaO		6.4%
Other oxides		5.9%

In spite of the lower cost of soda lime glass, the presence of oxides giving rise to insoluble products in larger quantities (as can be seen from Table 3-3) creates rougher etched channels when compared to borosilicate glass. The structural characteristics and also the excellent transmission make borosilicate glass an ideal choice for a wide range of applications in analytical and optical equipment. The Borofloat 33 glass has also been designed to withstand high temperatures up to 450° C for long periods, thus having high temperature stability.

3.2.2 Type of Etching and Etchants Used

We have etched both soda lime glass and borosilicate glass using wet etching. The etchants used for soda lime glass were 49% HF, nitric acid (HNO_3), and water (H_2O). After a series of experiments involving different proportions of the etchants for optimizing the etch depth and the surface roughness, the optimum etchant compositions for soda lime glass were found to be 3:2:25 (HF: HNO_3: H_2O) with an etch rate of 50-55 μm/hr and an average roughness value (R_a) varying from 5-10 nm as measured by the Tencor surface profilometer. The etchants used for borosilicate glass were 49% HF and hydrochloric acid (HCl) in proportions of 10:1 (HF: HCl). This ratio of HF:HCl is known

to have an optimal etch rate and surface roughness [100, 101]. The observed etch rate was around 5 μm/min with an average roughness value (R_a) of around 60 nm as measured by the Dektak surface profiler.

Roughness inside the etched microchannels is one of the factors affecting the selection of the type of substrate and also the etchants. Rough channel surfaces create unwanted fluorescence signals to the optical detection system. Since our microfluidic system is a fluorescence based optical detection system that detects the DNA amplification through the level of fluorescent signal received from the microchannels, the unwanted fluorescence due to the rough microchannels is undesired. Roughness also leads to the adsorption of molecules in the PCR mixture to the channel walls, thus disturbing fluid flow and causing loss of reagents. Few of the factors affecting the channel roughness are the type of substrate and the etchants used. The higher percentage of SiO_2+B_2O_3 content when compared to other oxides in borosilicate glass causes an increased etch rate and a decreased surface roughness [107]. The purpose in addition of HCl in the wet etching of glass is that the insoluble oxide products from glass formed after reaction with HF are converted into soluble products, thus resulting in smoother surfaces [100].

Figure 3-1 shows an example of the etch depth values inside a 115 μm etched chip as measured by the surface profiler. The roughness values inside the wide channels were measured to be around 1.5 μm. The channel width is also measured to be 750 μm and 350 μm between the top edges of the wide and the narrow channels respectively as opposed to the values (350 μm for wide and 30 μm for narrow channels) as per the designed mask. The widening of the channels is an unavoidable isotropic etch nature of

the wet etching. A single scan from the surface profiler instrument allows for the re-positioning of the cursors to obtain measurements such as etch depths, roughness values, and channel widths in the microchannels.

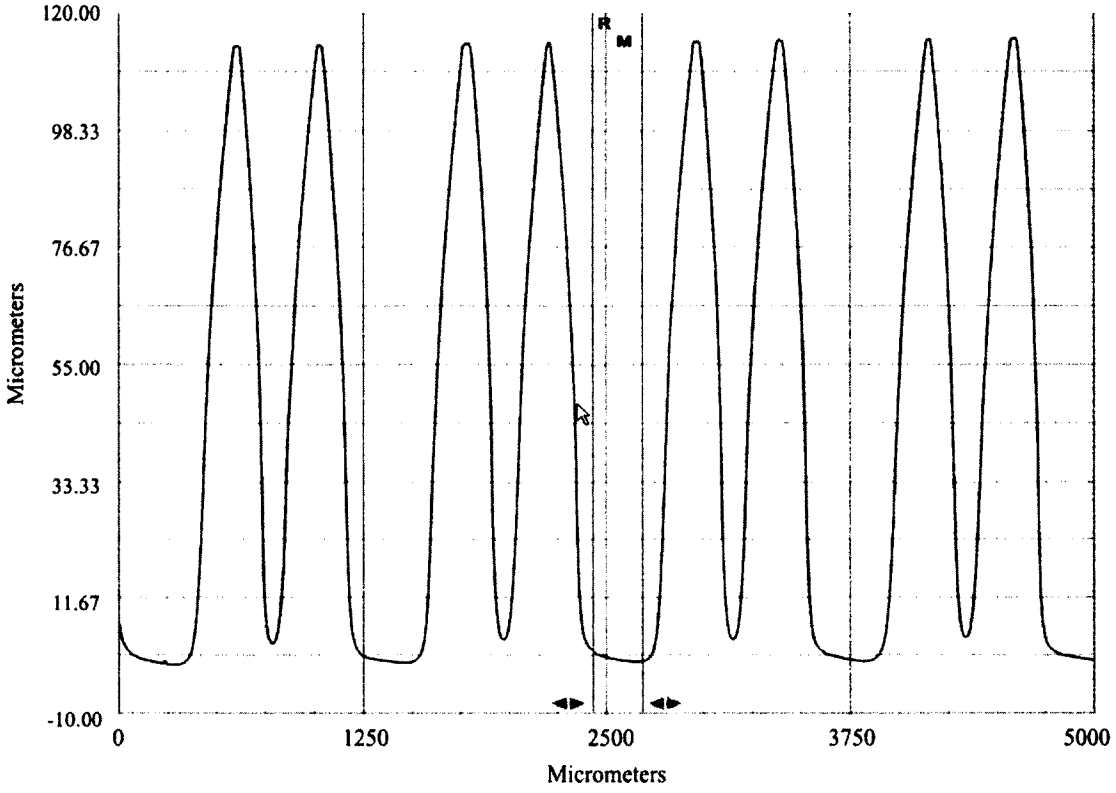

Figure 3-1: Etch depth measurement from the surface profiler.

3.2.3 Masking Layers and Mask Design

An important aspect in patterning glass substrates is choosing the masking layer during etching. Several masking layers for wet etching of glass have been reported such as photoresist, Chrome (Cr)/Gold (Au), Cr/photoresist, SU-8, amorphous silicon, silicon carbide, PECVD amorphous silicon, and LPCVD polysilicon [57, 100, 118-120]. The successful mask layers include multilayer depositions of Cr/Au with photoresist, low stress amorphous silicon/photoresist, and low stress amorphous silicon/low stress silicon

carbide/photoresist [57, 118]. The residual stress in the mask's layers (compressive or tensile) and the hydrophobicity play an important role in its functioning [121-123]. Defects in the masking layer can also lead to tensile stress and cracks in the layer, through which the HF solution seeps into, thus forming pinholes. A hydrophobic mask reduces the risk of the HF solution seeping through the defects in the mask. The hydrophobicity of hard-baked photoresist when used along with the other masking layers also reduces the penetration of HF through the defects in the mask [57].

L-edit software has been used to design the mask required for UV photolithography. The mask design that was transferred onto the substrate is shown in Figure 3-2. The mask is 125 mm X 125 mm in size with the pattern centered on it and the substrate is a circular wafer of 100 mm in diameter. The substrate can be directly placed in the substrate holder of the mask aligner during the photolithography without any orientation requirement with respect to the mask. With the initial glass substrate being a circular wafer, the laborious work of alignment of the mask with respect to the substrate is avoided. The three designs in a single mask allow the transfer of the complete mask pattern onto the circular glass substrate, which results in three separate glass devices upon dicing at the completion of fabrication. The pattern contains an inlet and an outlet with alternating wide and narrow serpentine channels. The wide channels allow the sample to have slower temperature ramp towards the denaturing temperatures (the hot end of the chip). The channels where temperature ramping is not necessary while the sample gets cooled down are narrow to allow rapid temperature changes.

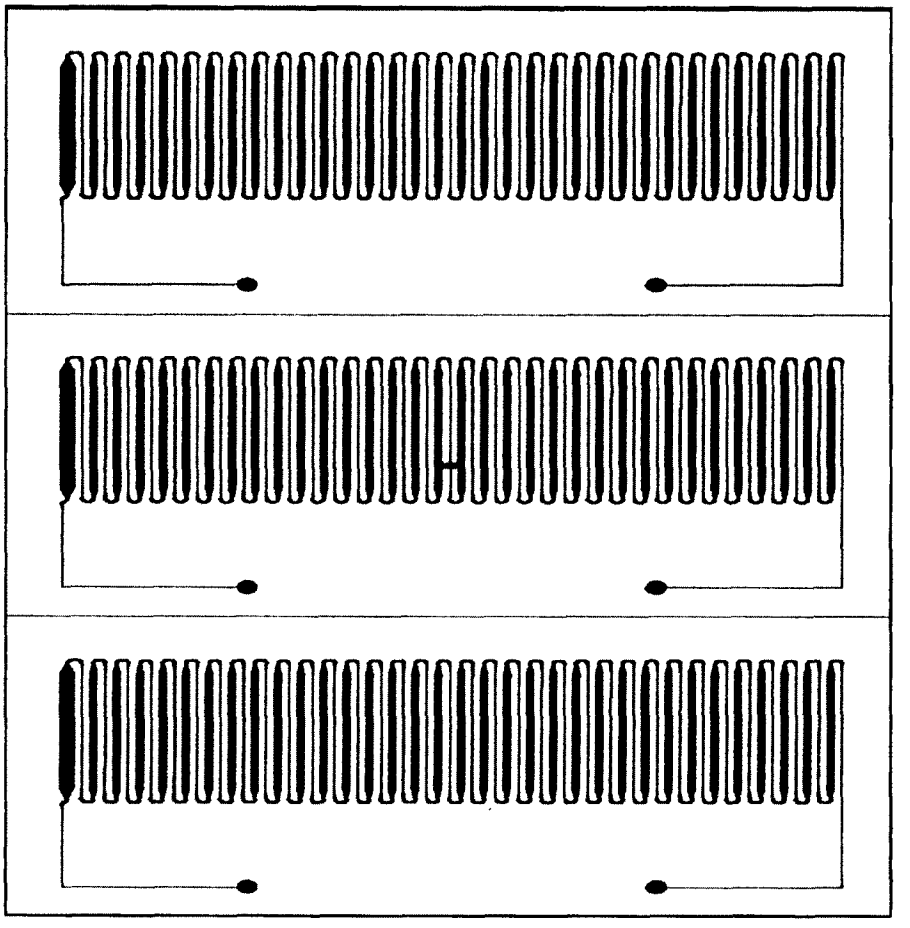

Figure 3-2: Fabrication mask design.

3.2.4 Steps Followed for Microchannel Fabrication

The procedure followed for fabricating microchannels in glass using photolithography and wet chemical etching is shown in Figure 3-3. The complete fabrication process is performed in a clean room environment.

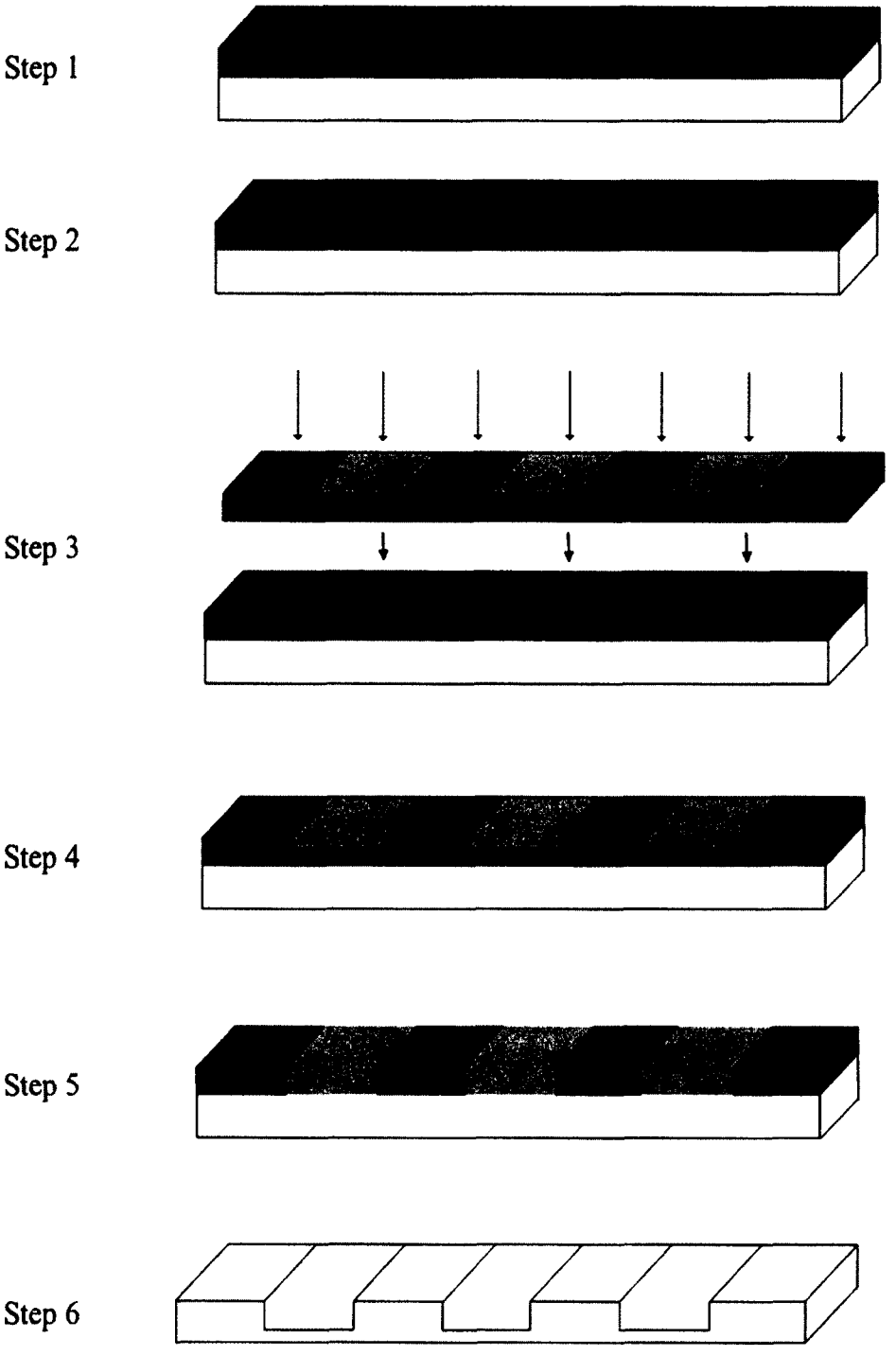

Figure 3-3: Steps for glass patterning.

Step 1: The substrate was initially annealed at 550° C for 5 hours. The annealing step causes redistribution of oxides in glass leading to a higher etch rate and also better surface quality [122, 123]. The substrate was then coated with layers of Cr/Au using sputtering. The thicknesses of the Cr and Au layers were 5 nm and 200 nm, respectively. The Cr layer is used as adhesion layers while the Au layer works as etch resistance layers.

Step 2: The substrate was hard-baked at 250° C for 20 minutes to drive off any solvents. A layer of positive photoresist was then spin-coated on the substrate to a thickness of 1 μm. The substrate was soft-baked for about 50-60 seconds at 115° C to remove solvents and avoid photoresist from sticking to the mask during exposure.

Step 3: The substrate was placed in a substrate holder under the mask and exposed to UV in a mask aligner for about 10 seconds. The UV rays that pass onto the substrate as per the designed mask cause photosolubilization of the exposed areas.

Step 4: The substrate was immersed into a developer solution, Microposit MF 319, for about 40-60 seconds. This causes the UV exposed regions of the photoresist on the substrate to get washed away. The pattern on the designed mask was transferred onto the photoresist layer on the substrate. The substrate was then hard-baked for about 10 minutes at 125° C. The hard-baking step was essential to resist easy penetration of the glass etchants through the photoresist.

Step 5: The substrate was immersed serially in Au and Cr etchants for 1.5-2 minutes and 1 minute, respectively. Au etchants, also called aqua regia, contains HNO_3: HCl (1:3). Cr etchants are typically a mixture of perchloric acid and ceric ammonium

nitrate. The substrate was then stripped off the photoresist, Au, and Cr layers in the required channel regions according to the designed mask.

Step 6: The substrate was submerged into the glass etchant mixture, HF: HCl (10:1) for 15 minutes resulting in an etch depth of 75 μm with an average roughness value (R_a) of around 65 nm. The substrate was then sprayed over with acetone to remove any remaining photoresist layer, followed by serial immersions in Au and Cr etchants to remove all the layers on the substrate surface. The final acquired substrate was a glass wafer with etched microchannels in it.

The substrate was then cleaned using a laboratory powdered contaminant-cleaning agent, 2% solution of Alconox (Alconox Inc., NY). Etch depth and the surface roughness measurements in the microchannels were obtained using a Dektak surface profiler. The circular glass substrate was then diced using a programmable wafer-dicing machine (Paxco Ind. Inc., TX) which resulted in three rectangular substrates having dimensions of 45 mm X 22.5 mm.

3.2.5 Steps Followed for Glass/glass Bonding

The bonding technique chosen involved the surface activation of substrates in a piranha solution composed of 3 parts of sulphuric acid (H_2SO_4) and 1 part of hydrogen peroxide (H_2O_2). It is well known that piranha solution clears off any organic residues on the substrates. Piranha has been used to successfully bond glass substrates at room temperatures [124, 125]. It modifies the surface chemistry of glass, rendering it to become hydrophilic by the formation of Si-OH groups on the surface. The hydrolyzed surfaces when put together for extended time periods, the Si-OH groups dehydrate, thus

forming siloxane bonds and terminating with a condensation-polymerization reaction as shown in Eq. 3.1 [108, 113, 126]:

$$Si - OH + OH - Si \rightarrow Si - O - Si + H_2O. \qquad \textbf{Eq. 3.1}$$

Following the fabrication of microchannels in the glass substrate and dicing, it needs to be bonded with another plain glass to form a sealed microfluidic device. The steps followed for glass/glass bonding as performed in a cleanroom are discussed in this subsection.

Step 1: The plain glass substrate was drilled with holes at the inlet and the outlet corresponding to the etched substrate pattern.

Step 2: Both glass substrates were cleaned with a laboratory glass-cleaning agent, Alconox (2% solution) to get rid of dust particles.

Step 3: Both glass substrates were then blown dry using a nitrogen gun and immersed in a container with piranha solution, H_2SO_4: H_2O_2 (3:1), for about 30 minutes. The piranha activates the surface of the soaked substrates by hydrolyzing them.

Step 4: The substrates taken out of the piranha solution were rinsed well in de-ionized (DI) water and pressed together carefully in the presence of running DI water such that no contaminants from the air came into contact with the bonding surfaces.

Step 5: The substrates were kept pressed together while we dried off the outer surfaces followed by placing them carefully in a substrate holder. A weight of about 15 lbs was placed on top of the substrates to ensure that they were in intimate contact with each other. The formation of the hydrolyzed layer in between the substrates allowed covalent bonding between them.

Step 6: The substrates were left in the holder under the weight for 5-6 hours. In case of any improper bonding with each other, the interference fringes (Newton's rings) were visible in the bonded substrates. In the presence of Newton's rings, the substrates were carefully tried to separate from each other and the bonding procedure was repeated from step 2.

Step 7: If the substrates look well-bonded, then they need to be bonded permanently. The substrates need to be annealed at least at low temperatures to undergo condensation reactions, thus forming permanent bonds with each other. In order to condense the silanol groups Si-OH to form permanent Si-O-Si, the bonded substrates were placed in a furnace that is heated up to 250° C for 2 hours. The substrate was removed from the furnace once it is cooled down and now the bonding of glass/glass is permanent to form a sealed microfluidic device.

3.2.6 Coating of Microchannels

The large surface-to-volume ratio in the microchannels necessitates focus on the surface characteristics such as roughness and compatibility with the biological samples used. Several surface passivation coatings have been investigated by research groups to create smooth channels for sample flow, to prevent reagent adsorption, and also avoiding any contaminants from the microfabrication process or stiction effects in the channels [127, 128]. We have chosen a chemical solution Pico-Glide^{TM} 1 (Dolomite Microfluidics, UK) to coat the microchannels. The coating procedure for Pico-Glide was followed as per the manufacturer's instructions from the catalog.

Step 1: The fabricated microdevice was exposed to oxygen plasma in a Technics micro-reactive ion etch (RIE) system for 5 minutes to activate the surface of the

microchannels. The plasma treatment activates the channel surface by creating hydroxyl groups rendering it hydrophilic.

Step 2: Immediately upon oxygen plasma treatment, the microchannels were filled-in with the Pico-Glide solution using an external pump at a flow rate of 2 μl/min.

Step 3: The filled-in microdevice was covered at the inlet and the outlet holes to prevent evaporation. The device was left at room temperature for 1 hour.

Step 4: The Pico-Glide was pulled back into the syringe out of the microchannels. The microchannels were then refilled with Fluorinert™ FC40 oil, which was later pulled back. The fluorophilic layer formed in the microchannels ensures improved droplet performance.

3.2.7 Experimental Set Up

The experimental set up showing the arrangement of the fabricated microdevice fixed onto the chip holder can be seen in Figure 3-4. The metal chip holder (Dolomite Microfluidics, UK) was supplied with holes for the tubing to be inserted at the inlet and the outlet holes on the chip. The microfluidic chip was screwed into the metal chip holder such that it maintains an airtight contact at the inlet and the outlet tubing/chip interface.

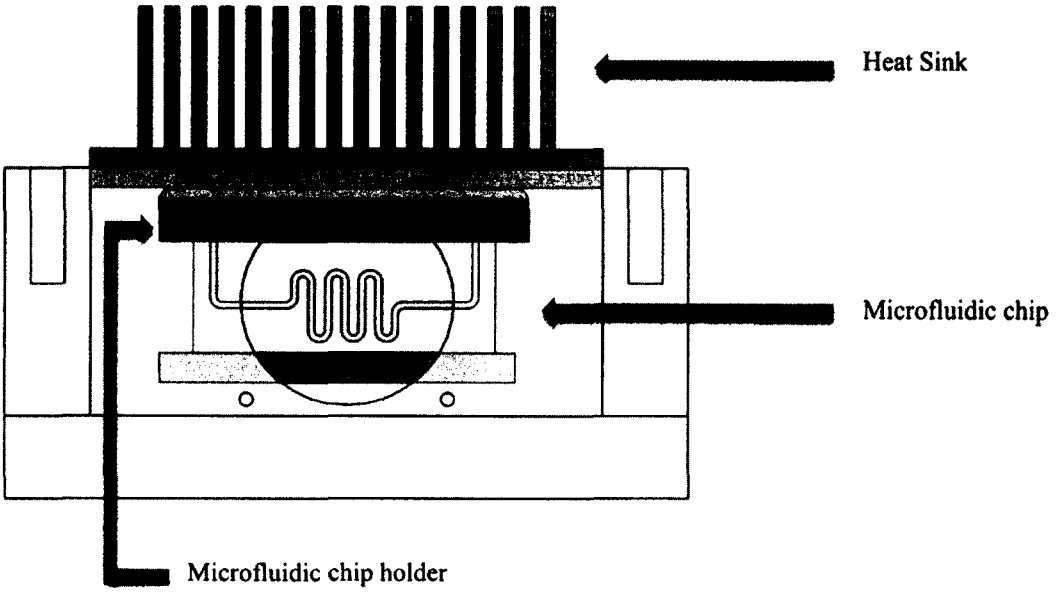

Figure 3-4: Experimental set up of the microfabricated chip.

A metal block was machined and attached to the edge of the microdevice parallel to the chip holder using a conductive tape. A linear temperature gradient was maintained across the microfluidic device by using a pair of heaters and thermocouples at the top and bottom edges of the microdevice, respectively. The heaters and the thermocouples were connected to a circuit board, which was remotely controlled using a computer with installed graphical user interface (GUI). The circuit board was connected to the computer using Bluetooth. A uniform temperature distribution across the microdevice plays an important role in the performance of on-chip PCR affecting the formation of the PCR product. An infrared camera was used initially to determine the set points required for the heaters in order to maintain the exact temperatures along the microchannels needed for on-chip PCR.

3.2.8 PCR Analysis

The PCR mixture was prepared with 0.48 ng/μl of DNA template, 0.5 μM of each of the forward and reverse primers, 1X buffer and 0.08 U/μL of enzyme mix (Takara Bio, Inc., Japan), 0.25 mg/ml BSA (Sigma-Aldrich, MO, USA), and 1X LCGreen. The primers amplified a 110-bp portion of the ΦX174 bacteriophage (New England Biolabs, MA, USA). From the prepared master mix of 120 μl, one sample of 10 μl was amplified on the LS32 as a control sample. The remaining PCR mixture was flown through the chip using an external pump at a flow rate of 0.5 μl/min. Once the chip was filled completely with the PCR mixture, the heaters were turned on. Since it takes approximately 7 minutes for the temperature gradient to be stabilized on the chip, after about 20 μl was flown, the sample out of the chip was collected in separate vials in 15 μl intervals. The collected sample was loaded into glass capillaries (LightCycler® Capillaries, Roche) to analyze in the LS32. Each capillary was loaded with 9 μl of the chip-flown mixture and 1 μl of the LCGreen dye. The samples were melted on the LS32 to determine the amplification on the chip.

3.3 Results and Discussion

3.3.1 Microfabrication

The fabricated glass/glass device used in these experiments is a 62 μm deep etched chip with a channel roughness of around 50 nm in the wide channel. The different curves/areas in the patterned substrate after developing of photoresist (at the end of photolithography) and prior to etching are shown in Figure 3-5.

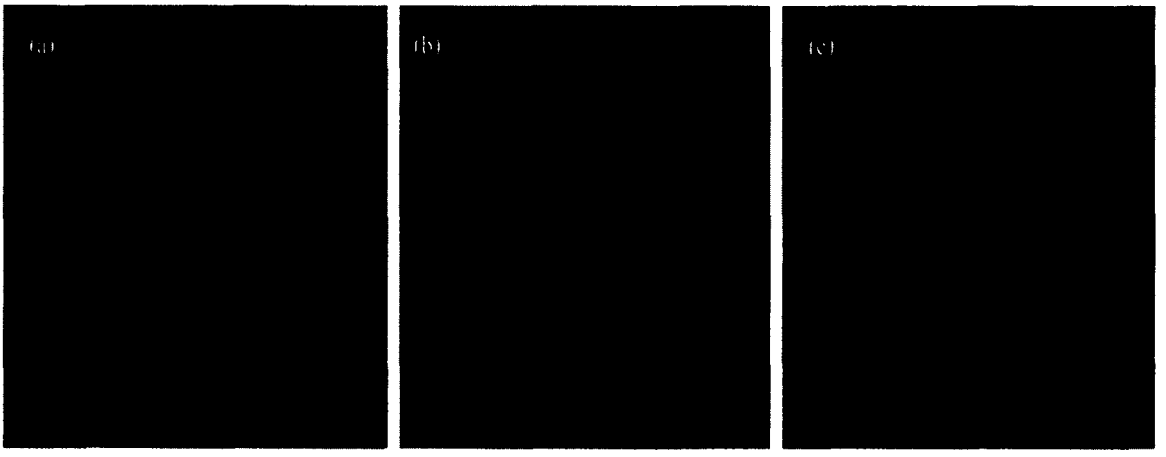

Figure 3-5: Microscopic view of the patterned channels on the chip prior to etching showing (a) a hot end of the channels when performing PCR, (b) a pair of the wide and the narrow channels in the center, and (c) a cool end of the channels.

The etching profile in the microchannels can be seen clearly from the microscopic image shown in Figure 3-6. The etched microchannels were measured for channel widths at the bottom and the top edges of the wide channel and the measurements are shown in Figure 3-6. The isotropic etch also caused the fusing of the channels with each other in the 115 μm deep etched chip.

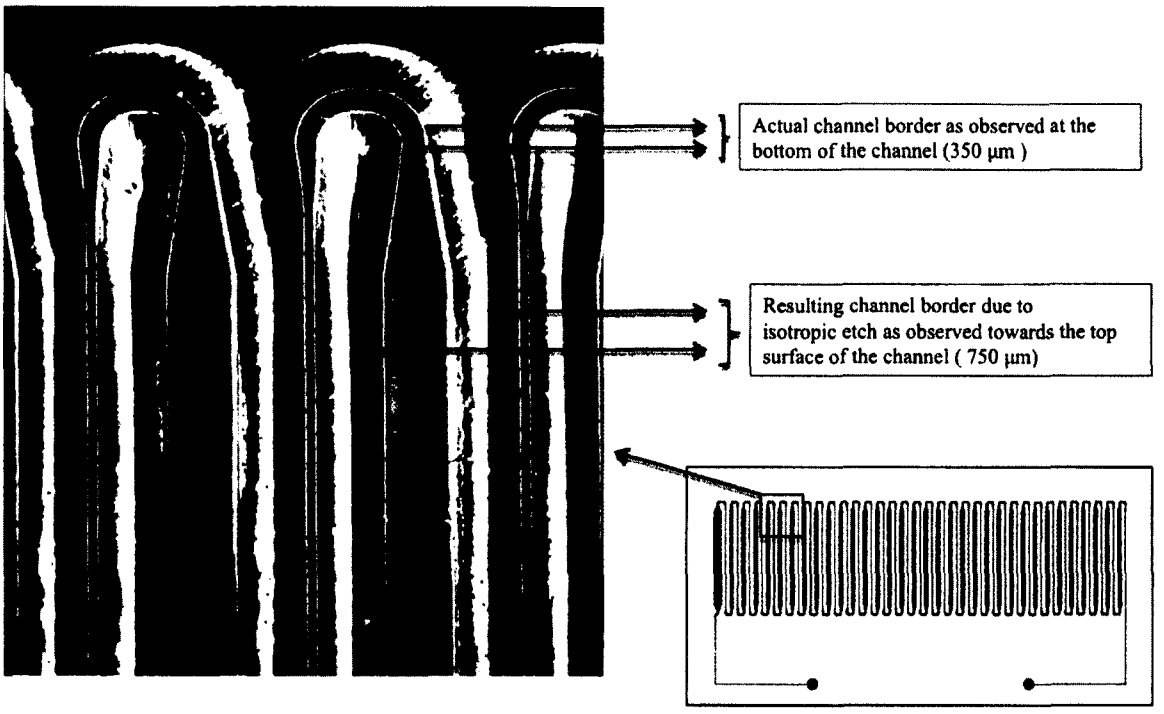

Figure 3-6: Etching profile in the microchannels of the 115 μm etched chip. The view of the isotropic etch in the channels is clear in the area surrounding all the channels.

The bonding yield of the glass/glass devices is 90%. The yield is dependent on various factors such as the cleanroom environment, the cleanliness of the substrate prior to surface activation by piranha, and the application of the required pressure to keep the substrates close for easier formation of silanol bonds between them. The improper bonding between the glass substrates results in interference fringes as shown in Figure 3-7. The interference fringes observed are a result of the reflection of the light from the interface between the substrates, which is an indication of the weak bonding between the bonded substrates.

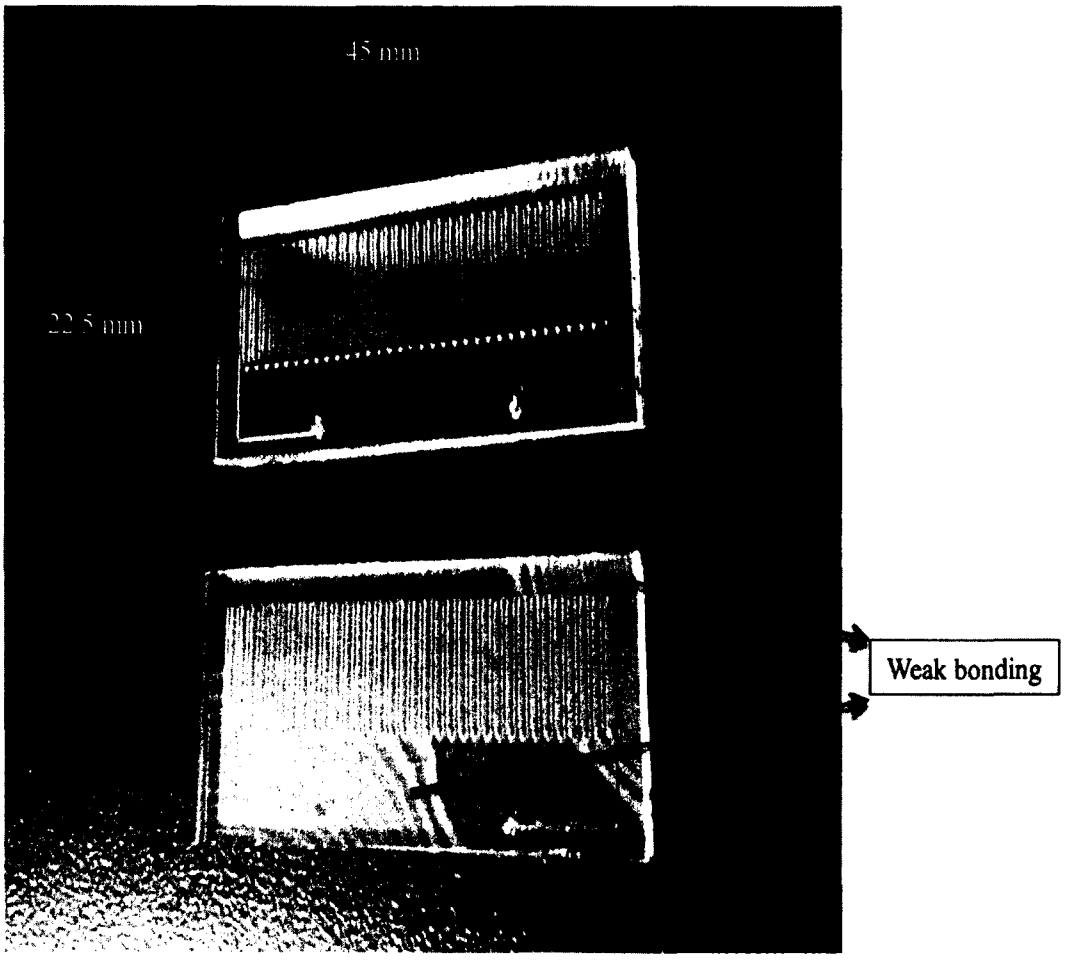

Figure 3-7: Perfectly bonded device (top) and improper bonding showing interference fringes (bottom).

3.3.2 On-chip Microfluidics

The total volume of the 62 μm deep etched chip is about 16 μl. The flow rate used in this chip is 0.5 μl/min resulting in a cycle time of 1 minute. The channel height in the chip is 11 mm. The temperatures as measured by the infrared camera on the top and the bottom of the channels are 95 and 60° C. The cycle time for the wide channel is about 45 seconds which is translated to a heating rate of 0.8° C/s. The cycle time for the narrow channel of about 15 seconds is translated to a cooling rate of 2.3° C/s.

The chip-amplified samples were also melted on the LS32 and we compared them with the LS32 amplified control sample. Figure 3-8 shows the melt curve and peak of the LS32 amplified sample.

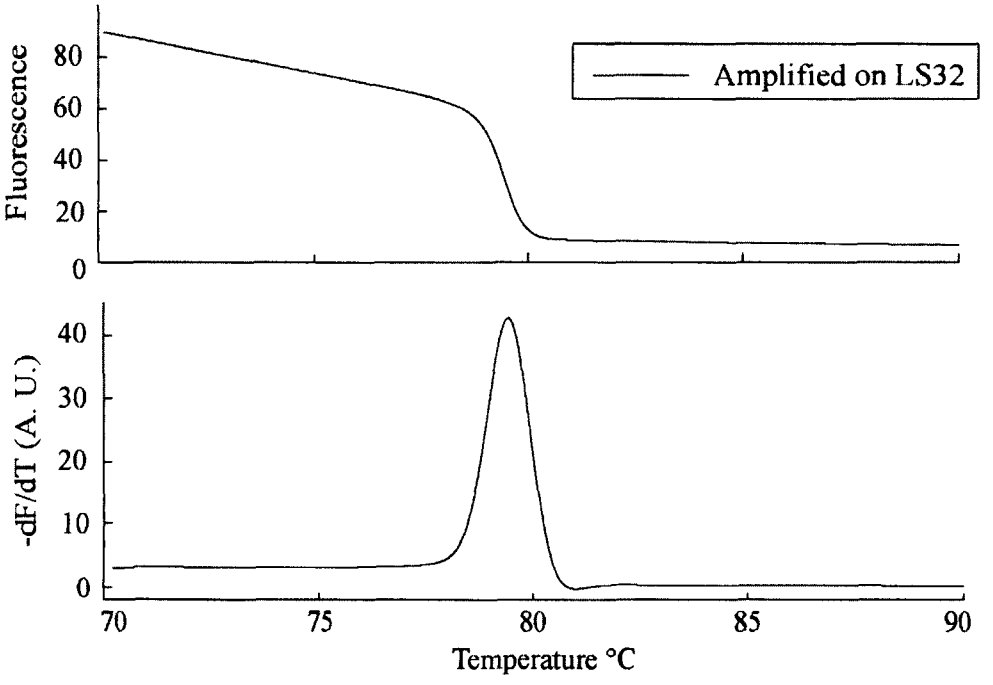

Figure 3-8: The melt curve and melt peak of an aliquot from the bulk PCR mixture amplified in the LS32 as a control sample is shown.

From the remaining bulk PCR mixture flown through the chip, the samples were collected from the outlet in 15 μl intervals. Figure 3-9 shows the melt curves and peaks of the chip-amplified samples, in which the samples were numbered in the order they were collected from the chip.

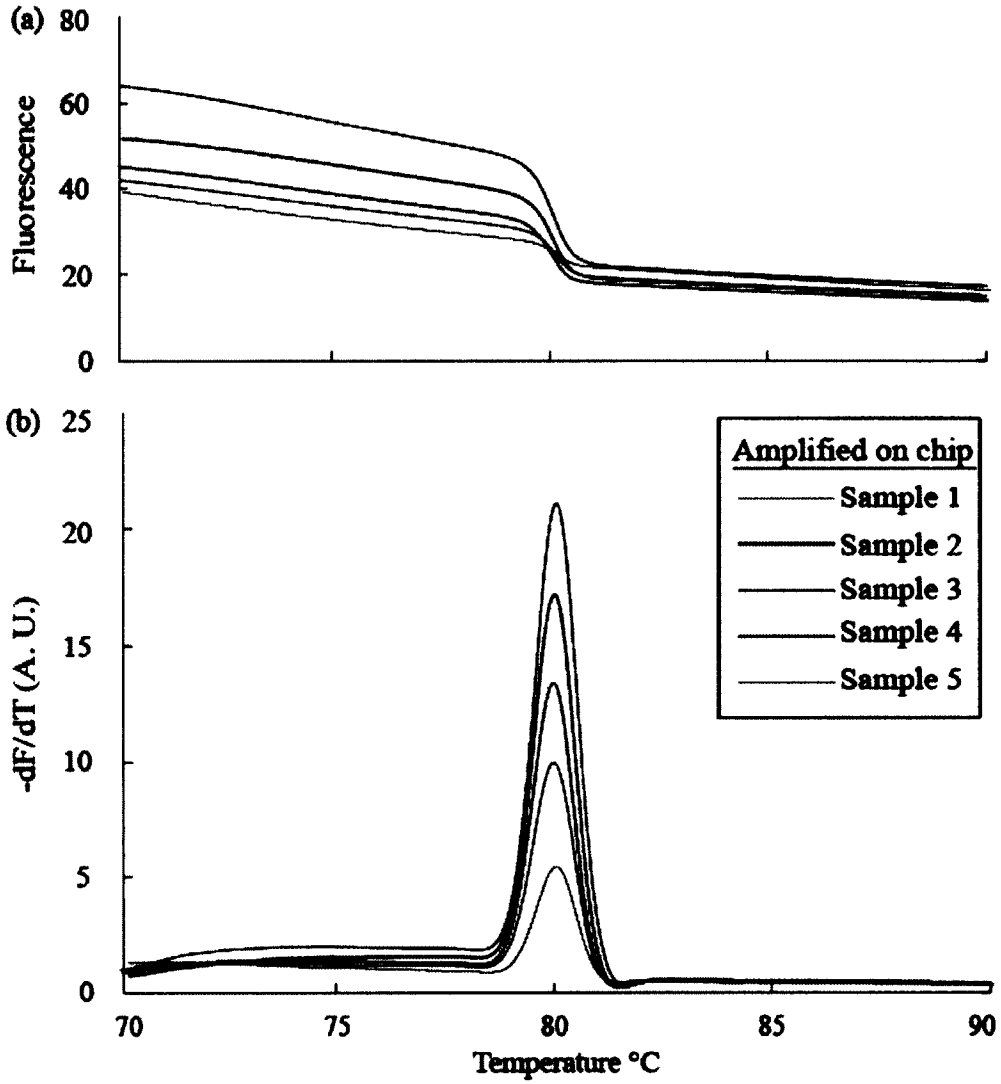

Figure 3-9: The samples are numbered in the legend in the order they were collected from the chip. Sample 1 is collected after 35 µl was flown through the chip and the rest of the samples were collected in 15 µl intervals.

The comparison between the melting peaks from Figure 3-8 and Figure 3-9 indicates the amplification of the specific 110-bp product and no non-specific amplification (primer dimers). It was observed from the melts of the chip-flown samples that the amplification product increased with time, and after a certain time, it gradually decreased. Since the chip was initially filled-in with the PCR mixture and then the heaters

were turned on, the initial samples collected from the chip would have flown through less number of temperature cycles resulting in a lesser product. This accounts for the increase in the product between the samples 1, 2, and 3. After the collection of sample 3, the product decreased again gradually. This decrease can be attributed to several factors such as an unstable temperature gradient along the channels over time, the clogging inside the channels because of the addition of BSA to the PCR mixture, also any channel coating particulates (from picoglide) inhibiting PCR after extended use of the chip at high temperatures. Nevertheless, the microfluidic set up has been successfully validated in terms of performance of rapid PCR.

3.4 Conclusions

This work has mainly focused on the microfabrication of a glass-to-glass bonded device to analyze DNA. We have successfully fabricated a glass/glass microdevice and investigated the performance of on-chip rapid PCR in a cycle time of 1 minute for both the heating and the cooling phases together. The fabrication steps included photolithography, wet etching and bonding to form the microfluidic device. We have used the Pico-Glide coating to passivate the channel surface in order to reduce the reagent adsorption and create a smooth flow throughout the microchannels. The surface passivation can be further investigated to ensure its compatibility with the temperatures and the protocol used in these experiments. While the experiments in this work used an arbitrarily chosen flow rate of 0.5 μl/min, a higher flow rate can be used to decrease the cycle time needed for amplification. The integration of the microfluidic system with high-resolution CCD camera optics will provide high-resolution images. This will enable the analysis of fluorescence data collected directly from the chip. This will eliminate the

steps followed in this current work for sample collection from the chip and analysis on the conventional instrument. To summarize, the integrated microfluidic system possesses the capability of real-time analysis of genetic changes in the DNA including a rapid and an efficient damage analysis system. The micro-scale consumption of the reagents, the short reaction times, high throughput, and the portability of the entire integrated microfluidic system prove advantageous in a wide variety of areas such as clinical, biological, and pharmaceutical industries.

CHAPTER 4

CONCLUSIONS AND FUTURE WORK

4.1 Conclusions

This chapter summarizes the results obtained on the conventional instrument and the on-chip microfluidics. The future prospects of the work presented here by possible further experimentation/integration of several variables is also discussed.

4.1.1 Summary of Findings on Conventional Instrumentation

We have successfully performed real-time monitoring of biological changes in DNA using fluorescence-based techniques on an existing instrumentation. In order to create the biological changes, we have created known damage to DNA in several forms at the intramolecular level as well as strand breaks. Simplified damage models were used in these experiments: UV-C irradiation to produce photoproducts, and restriction enzyme digestion to simulate double-strand breaks. The techniques applied in this work, qPCR and HRMA have been demonstrated successfully to distinguish the difference between different levels of damaged DNA samples. A reliable quantification of DNA damaged prior to amplification has been performed using qPCR. HRMA has also been shown as an efficient closed-tube, sensitive and non-destructive sequential analysis to PCR without the need of additional instrumentation. Our work here represents the first time that HRMA has been used to measure DNA damage induced by radiation. We have compared this technique with the conventional amplicon analysis system, gel electrophoresis, and

proven it to be much more sensitive at the detection of these genetic changes in DNA. While gel electrophoresis poses problems in distinguishing between amplicons of similar lengths, HRMA can be used to accurately differentiate between different products based on their melting behavior (which is sequence-dependent). The findings of this work, however, can be intuitively applied to the broad scope of DNA damage mechanisms. The simplicity, sensitivity and the specificity of these techniques offer a wide variety of applications ranging from medical diagnostics to forensic science.

4.1.2 Summary of Findings on Microfluidic System

The ability to perform rapid PCR on a microfluidic chip has been demonstrated in this work. We have been able to pattern and fabricate a borosilicate glass microdevice with minimal etch defects. Wet chemical etching has been used to fabricate the microchannels with aspect ratios (depth to width ratio considering the width at the top edge of the channels) of about 0.18 in the wide channels and 0.38 in the narrow channels in a 115 μm deep etched glass substrate. We have been successful in bonding glass-to-glass through surface activation (using piranha) and annealing the substrates at low temperatures. To our knowledge, no one has reported permanent glass/glass bonding of borosilicate substrates at a temperature as low as 250° C in a short time of 8-10 hours. We have tested the bonding between the glass substrates at different flow rates ranging from 0.5-4 μl/min and the bonded chip remained intact without any leakage. The microdevice has been able to perform rapid PCR with a cycle time of 1 min (combining both the heating and the cooling cycles). The fabricated device has been integrated with a pair of heaters and thermocouples to set up a micro-PCR device, which can also be

integrated with a high quality CCD camera to observe the amplification or genetic changes in DNA in real-time.

4.1.3 Conventional Instrumentation versus Microfluidic System

The microfabricated system for PCR offers the possibility of portable devices that can be of great use in medical and biological applications. The major limiting factor for the speed of PCR is the capability of fast temperature changes and the heat exchange between the device and the sample. The reduction in thermal mass in the microfluidic system when compared to the conventional instruments allows rapid thermocycling and lower power consumption. The other advantages of the microfluidic system include reduction in sample volumes used, decreased analysis time, and the possibility of integration of multiple components in the microdevice.

4.2 Future Work

A variety of improvements can be made involving different factors. A few possible modifications/additions to the existing work have been pointed out for an improvised system.

4.2.1 Improvements in Fabrication

Since deeper channels give rise to an increased volume of PCR mixture per each microchannel, the fluorescence signal emitted would increase making it easy for real-time on-chip qPCR and HRMA. The slight improvements needed in the fabrication process to accommodate the channel depth and increase the fluorescence signal are discussed in the following sub-section.

4.2.1.1 *Revised Mask Design*

The spacing between the channels used in this work is 400 μm. Since wet etching has been performed, the isotropic nature of the etch narrows the spacing between the channels. When deeper etching (~100 μm) was performed, some of the channels nearly fused with each other. Channel fusing has been noted from the surface profiler measurements and also when looked under the microscope (the spacing between the channels looked merely like a line rather than a flat edge). An increase in the spacing between the channels provides scope for deeper channels to avoid the risk of channels fusing with each other.

4.2.1.2 *Increased Mask Thickness*

The Cr/Au (5 nm/200 nm) mask used in this work was not found to be intact when taken out of the HF solution after 15 minutes of etching. Thicker layers of Cr/Au (60 nm/400 nm) will need to be deposited to facilitate deeper etching (~100 μm). Also, multilayers in the sequence Cr/Au/Cr/Au can be deposited if the 60 nm/400 nm is still not found to be intact when removed from the HF solution.

4.2.2 Potential Directions

4.2.2.1 *On-chip qPCR*

The importance of qPCR in terms of sensitivity and reliable quantitation of nucleic acids has been discussed in this work. Unlike the conventional PCR, the ability of the real-time qPCR to monitor the accumulating products allows quantitation while in the exponential phase of the PCR. The integration of the currently developed microfluidic system with high quality optics will enable fluorescence-based detection of nucleic acids. Fluorescence-based signals extracted from a single image during the continuous-flow on-

chip PCR can be used to analyze both the qPCR and the DNA melting curves. By extracting fluorescence signal across the channels in the chip, qPCR can be performed by making use of the change in fluorescence with respect to the cycle numbers. The melting curve can be obtained by extracting the fluorescence signal in a single channel with respect to the temperature distribution in it. Although qPCR in the conventional instruments allows real-time monitoring of the generated amplicon, it does not offer the flexibility of choosing to analyze the amplified DNA during the amplification process or while the instrument is still running the sequential analyses after PCR. The advantage offered by microfluidic PCR is that simultaneous and also selective channel analysis (generating both the amplification data and the DNA melting curves) can be performed during the amplification.

4.2.2.2 *On-chip Multiplex PCR*

It has been proven in this work that multiplex PCR can be performed on the conventional instrumentation. The ability of the conventional instrument to identify differences in the damage between the DNA exposed to varying radiation exposure time has been shown in Chapter 2. However, of the two different products, namely the high risk and the low risk amplified in the multiplex reaction, the conventional instrument was able to observe the damage in just the high risk sequence. The reason for not being able to identify the damage in the low risk sequence is that it amplified to the maximum extent reaching the plateau phase in its amplification cycle because of which all the damaged and the undamaged portions of the low risk sequence showed the same product in the melting curves (since the difference between the damaged and the undamaged samples can be quantified using melting curves when only the reaction is stopped in the

exponential phase of the PCR). This issue can be overcome easily using on-chip multiplex PCR since it is convenient to extract fluorescence data from any of the channels desired from several images collected during the amplification. Though we have focused on detection of damages in multiplex PCR in this particular work, just the detection of multiplex PCR will be of great advantage in distinguishing several products in a single reaction mixture, thus minimizing the overall reagent cost, sample volumes, and it is also labor and time-effective.

4.2.2.3 *Replacing the External Pump*

The external pump currently used in this work is heavy and bulky posing a problem to the portability of the microfluidic system. Microfluidic devices fabricated from glass can make use of electrokinetic phenomena for pumping and sample flow in the microchannels. Incorporating electro-osmotic flow [91] induced pumping reduces the space requirements of the microfluidic system and also benefits convenience in operation due to the miniaturization.

4.2.2.4 *Integration of Cellular Analysis Components*

An ideal microanalysis system should possess features such as integration with components like cell isolation, ability to accept crude biological samples such as blood, capable to extract DNA/RNA, amplify the DNA by overcoming any PCR inhibitors, and be efficient enough to distinguish the products. Cell handling is one of the critical aspects to be considered in on-chip microfluidics. The scaling feature in microfluidics should provide a favorable and stable local microenvironment for cell culture. Integration of cell culture systems can be an advantage, in that growth can be controlled easily in the microenvironment rather than the culture flasks. This would also allow analysis at the

cellular level, thus providing a deeper insight for various biological applications.

In summary, fluorescence-based techniques/tools have been developed for the real-time DNA damage quantification using conventional laboratory instrumentation. We have demonstrated the ability of our microfluidic system to amplify DNA. The techniques demonstrated in this work on the conventional instrument can be extended and applied to the integrated microfluidic system to develop a more cost and time-sensitive approach to analysis of biological changes in real-time.

REFERENCES

[1] J.-L. Ravanat, T. Douki, and J. Cadet, "Direct and indirect effects of UV radiation on DNA and its components," *Journal of Photochemistry and Photobiology B: Biology,* vol. 63, pp. 88-102, 2001.

[2] S. Kumari, R. P. Rastogi, K. L. Singh, S. P. Singh, and R. P. Sinha, "DNA damage: detection strategies," *EXCLI J,* vol. 7, pp. 44-62, 2008.

[3] B. M. Sutherland, P. V. Bennett, O. Sidorkina, and J. Laval, "Clustered DNA damages induced in isolated DNA and in human cells by low doses of ionizing radiation," *Proceedings of the National Academy of Sciences,* vol. 97, pp. 103-108, 2000.

[4] A. Sancar, L. A. Lindsey-Boltz, K. Ünsal-Kaçmaz, and S. Linn, "Molecular mechanisms of mammalian DNA repair and the DNA damage checkpoints," *Annual review of biochemistry,* vol. 73, pp. 39-85, 2004.

[5] Y. Zhang and P. Ozdemir, "Microfluidic DNA amplification—a review," *Analytica chimica acta,* vol. 638, pp. 115-125, 2009.

[6] C.-S. J. Hou, M. Godin, K. Payer, R. Chakrabarti, and S. R. Manalis, "Integrated microelectronic device for label-free nucleic acid amplification and detection," *Lab on a Chip,* vol. 7, pp. 347-354, 2007.

[7] L. Betelli, P. Duquenne, F. Grenouillet, X. Simon, E. Scherer, E. Géhin, and A. Hartmann, "Development and evaluation of a method for the quantification of airborne Thermoactinomyces vulgaris by real-time PCR," *Journal of microbiological methods,* 2012.

[8] K. M. Ririe, R. P. Rasmussen, and C. T. Wittwer, "Product differentiation by analysis of DNA melting curves during the polymerase chain reaction," *Analytical biochemistry,* vol. 245, pp. 154-160, 1997.

[9] J. Ward, J. Evans, C. Limoli, and P. Calabro-Jones, "Radiation and hydrogen peroxide induced free radical damage to DNA," *The British journal of cancer. Supplement,* vol. 8, p. 105, 1987.

[10] T. Yagura, K. Makita, H. Yamamoto, C. F. Menck, and A. P. Schuch, "Biological sensors for solar ultraviolet radiation," *Sensors,* vol. 11, pp. 4277-4294, 2011.

[11] T. Douki, A. Reynaud-Angelin, J. Cadet, and E. Sage, "Bipyrimidine photoproducts rather than oxidative lesions are the main type of DNA damage involved in the genotoxic effect of solar UVA radiation," *Biochemistry,* vol. 42, pp. 9221-9226, 2003.

[12] J. Cadet, S. Courdavault, J.-L. Ravanat, and T. Douki, "UVB and UVA radiation-mediated damage to isolated and cellular DNA," *Pure and applied chemistry,* vol. 77, pp. 947-961, 2005.

[13] D. Perdiz, P. Gróf, M. Mezzina, O. Nikaido, E. Moustacchi, and E. Sage, "Distribution and Repair of Bipyrimidine Photoproducts in Solar UV-irradiated Mammalian Cells POSSIBLE ROLE OF DEWAR PHOTOPRODUCTS IN SOLAR MUTAGENESIS," *Journal of Biological Chemistry,* vol. 275, pp. 26732-26742, 2000.

[14] J. M. Song, J. Milligan, and B. M. Sutherland, "Bistranded oxidized purine damage clusters: induced in DNA by long-wavelength ultraviolet (290-400 nm) radiation?," *Biochemistry,* vol. 41, pp. 8683-8688, 2002.

[15] A. Kumar, M. B. Tyagi, and P. N. Jha, "Evidences showing ultraviolet-B radiation-induced damage of DNA in cyanobacteria and its detection by PCR assay," *Biochemical and biophysical research communications,* vol. 318, pp. 1025-1030, 2004.

[16] T. Douki and J. Cadet, "Individual determination of the yield of the main UV-induced dimeric pyrimidine photoproducts in DNA suggests a high mutagenicity of CC photolesions," *Biochemistry,* vol. 40, pp. 2495-2501, 2001.

[17] H. Wei, Q. Ca, R. Rahn, X. Zhang, Y. Wang, and M. Lebwohl, "DNA structural integrity and base composition affect ultraviolet light-induced oxidative DNA damage," *Biochemistry,* vol. 37, pp. 6485-6490, 1998.

[18] K. Cahová-Kucharíková, M. Fojta, T. Mozga, and E. Paleček, "Use of DNA repair enzymes in electrochemical detection of damage to DNA bases in vitro and in cells," *Analytical chemistry,* vol. 77, pp. 2920-2927, 2005.

[19] D. P. Kalinowski, S. Illenye, and B. Van Houten, "Analysis of DNA damage and repair in murine leukemia L1210 cells using a quantitative polymerase chain reaction assay," *Nucleic acids research,* vol. 20, pp. 3485-3494, 1992.

[20] K. Rudi, I. Hagen, B. C. Johnsrud, G. Skjefstad, and I. Tryland, "Different length (DL) qPCR for quantification of cell killing by UV-induced DNA damage," *International journal of environmental research and public health,* vol. 7, pp. 3376-3381, 2010.

[21] D. Jung, Y. Cho, J. N. Meyer, and R. T. Di Giulio, "The long amplicon quantitative PCR for DNA damage assay as a sensitive method of assessing DNA damage in the environmental model, Atlantic killifish (Fundulus heteroclitus)," *Comparative Biochemistry and Physiology Part C: Toxicology & Pharmacology,* vol. 149, pp. 182-186, 2009.

[22] R. P. Rastogi, A. Kumar, M. B. Tyagi, and R. P. Sinha, "Molecular mechanisms of ultraviolet radiation-induced DNA damage and repair," *Journal of nucleic acids,* vol. 2010, 2010.

[23] O. Aruoma, B. Halliwell, E. Gajewski, and M. Dizdaroglu, "Damage to the bases in DNA induced by hydrogen peroxide and ferric ion chelates," *Journal of Biological Chemistry,* vol. 264, pp. 20509-20512, 1989.

[24] A. L. Miranda-Vilela, P. C. Alves, A. K. Akimoto, G. S. Lordelo, C. A. Gonçalves, C. K. Grisolia, and M. N. Klautau-Guimarães, "Gene polymorphisms against DNA damage induced by hydrogen peroxide in leukocytes of healthy humans through comet assay: a quasi-experimental study," *Environ Health,* vol. 9, p. 21, 2010.

[25] H. Willers, J. Dahm-Daphi, and S. Powell, "Repair of radiation damage to DNA," *British journal of cancer,* vol. 90, pp. 1297-1301, 2004.

[26] M. S. Cooke, M. D. Evans, M. Dizdaroglu, and J. Lunec, "Oxidative DNA damage: mechanisms, mutation, and disease," *The FASEB Journal,* vol. 17, pp. 1195-1214, 2003.

[27] H. Stone and S. Kim, "Microfluidics: basic issues, applications, and challenges," *AIChE Journal,* vol. 47, pp. 1250-1254, 2001.

[28] J. Chen, D. Chen, Y. Xie, T. Yuan, and X. Chen, "Progress of Microfluidics for Biology and Medicine," *Nano-Micro Letters,* vol. 5, 2013.

[29] P. N. Nge, C. I. Rogers, and A. T. Woolley, "Advances in microfluidic materials, functions, integration, and applications," *Chemical reviews,* vol. 113, pp. 2550-2583, 2013.

[30] G. S. Fiorini and D. T. Chiu, "Disposable microfluidic devices: fabrication, function, and application," *BioTechniques,* vol. 38, pp. 429-446, 2005.

[31] C. Zhang and D. Xing, "Single-molecule DNA amplification and analysis using microfluidics," *Chemical reviews,* vol. 110, pp. 4910-4947, 2010.

[32] J. A. Kim, J. Y. Lee, S. Seong, S. H. Cha, S. H. Lee, J. J. Kim, and T. H. Park, "Fabrication and characterization of a PDMS–glass hybrid continuous-flow PCR chip," *Biochemical engineering journal,* vol. 29, pp. 91-97, 2006.

[33] I. K. Dimov, J. L. Garcia-Cordero, J. O'Grady, C. R. Poulsen, C. Viguier, L. Kent, P. Daly, B. Lincoln, M. Maher, and R. O'Kennedy, "Integrated microfluidic tmRNA purification and real-time NASBA device for molecular diagnostics," *Lab on a Chip,* vol. 8, pp. 2071-2078, 2008.

[34] P. Wilding, M. A. Shoffner, and L. J. Kricka, "PCR in a silicon microstructure," *Clinical Chemistry,* vol. 40, pp. 1815-1818, 1994.

[35] A. Gulliksen, L. Solli, F. Karlsen, H. Rogne, E. Hovig, T. Nordstrøm, and R. Sirevåg, "Real-time nucleic acid sequence-based amplification in nanoliter volumes," *Analytical chemistry,* vol. 76, pp. 9-14, 2004.

[36] J. Khandurina, T. E. McKnight, S. C. Jacobson, L. C. Waters, R. S. Foote, and J. M. Ramsey, "Integrated system for rapid PCR-based DNA analysis in microfluidic devices," *Analytical Chemistry,* vol. 72, pp. 2995-3000, 2000.

[37] H. Wang, J. Chen, L. Zhu, H. Shadpour, M. L. Hupert, and S. A. Soper, "Continuous flow thermal cycler microchip for DNA cycle sequencing," *Analytical chemistry,* vol. 78, pp. 6223-6231, 2006.

[38] T. Fukuba, T. Yamamoto, T. Naganuma, and T. Fujii, "Microfabricated flow-through device for DNA amplification—towards in situ gene analysis," *Chemical Engineering Journal,* vol. 101, pp. 151-156, 2004.

[39] M. U. Kopp, A. J. De Mello, and A. Manz, "Chemical amplification: continuous-flow PCR on a chip," *Science,* vol. 280, pp. 1046-1048, 1998.

[40] H. Nakano, K. Matsuda, M. Yohda, T. Nagamune, I. Endo, and T. Yamane, "High speed polymerase chain reaction in constant flow," *Bioscience, biotechnology, and biochemistry,* vol. 58, p. 349, 1994.

[41] N. A. Friedman and D. R. Meldrum, "Capillary tube resistive thermal cycling," *Analytical chemistry,* vol. 70, pp. 2997-3002, 1998.

[42] J. Chiou, P. Matsudaira, A. Sonin, and D. Ehrlich, "A closed-cycle capillary polymerase chain reaction machine," *Analytical chemistry,* vol. 73, pp. 2018-2021, 2001.

[43] N. Crews, C. Wittwer, and B. Gale, "Continuous-flow thermal gradient PCR," *Biomedical microdevices,* vol. 10, pp. 187-195, 2008.

[44] I. Schneegaß, R. Bräutigam, and J. M. Köhler, "Miniaturized flow-through PCR with different template types in a silicon chip thermocycler," *Lab on a Chip,* vol. 1, pp. 42-49, 2001.

[45] K. Sun, A. Yamaguchi, Y. Ishida, S. Matsuo, and H. Misawa, "A heater-integrated transparent microchannel chip for continuous-flow PCR," *Sensors and Actuators B: Chemical,* vol. 84, pp. 283-289, 2002.

[46] P. J. Obeid, T. K. Christopoulos, H. J. Crabtree, and C. J. Backhouse, "Microfabricated device for DNA and RNA amplification by continuous-flow polymerase chain reaction and reverse transcription-polymerase chain reaction with cycle number selection," *Analytical chemistry,* vol. 75, pp. 288-295, 2003.

[47] P. J. Obeid and T. K. Christopoulos, "Continuous-flow DNA and RNA amplification chip combined with laser-induced fluorescence detection," *Analytica Chimica Acta,* vol. 494, pp. 1-9, 2003.

[48] T. Nakayama, Y. Kurosawa, S. Furui, K. Kerman, M. Kobayashi, S. R. Rao, Y. Yonezawa, K. Nakano, A. Hino, and S. Yamamura, "Circumventing air bubbles in microfluidic systems and quantitative continuous-flow PCR applications," *Analytical and bioanalytical chemistry,* vol. 386, pp. 1327-1333, 2006.

[49] S. Li, D. Y. Fozdar, M. F. Ali, H. Li, D. Shao, D. M. Vykoukal, J. Vykoukal, P. N. Floriano, M. Olsen, and J. T. McDevitt, "A continuous-flow polymerase chain reaction microchip with regional velocity control," *Microelectromechanical Systems, Journal of,* vol. 15, pp. 223-236, 2006.

[50] Y. Sun, Y. C. Kwok, and N.-T. Nguyen, "A circular ferrofluid driven microchip for rapid polymerase chain reaction," *Lab on a Chip,* vol. 7, pp. 1012-1017, 2007.

[51] M. Hashimoto, F. Barany, F. Xu, and S. A. Soper, "Serial processing of biological reactions using flow-through microfluidic devices: coupled PCR/LDR for the detection of low-abundant DNA point mutations," *Analyst,* vol. 132, pp. 913-921, 2007.

[52] O. Frey, S. Bonneick, A. Hierlemann, and J. Lichtenberg, "Autonomous microfluidic multi-channel chip for real-time PCR with integrated liquid handling," *Biomedical Microdevices,* vol. 9, pp. 711-718, 2007.

[53] L. Gui and C. L. Ren, "Numeric simulation of heat transfer and electrokinetic flow in an electroosmosis-based continuous flow PCR chip," *Analytical chemistry,* vol. 78, pp. 6215-6222, 2006.

[54] S. Zeng, C.-H. Chen, J. C. Mikkelsen Jr, and J. G. Santiago, "Fabrication and characterization of electroosmotic micropumps," *Sensors and Actuators B: Chemical,* vol. 79, pp. 107-114, 2001.

[55] J. Chen, M. Wabuyele, H. Chen, D. Patterson, M. Hupert, H. Shadpour, D. Nikitopoulos, and S. A. Soper, "Electrokinetically synchronized polymerase chain reaction microchip fabricated in polycarbonate," *Analytical chemistry,* vol. 77, pp. 658-666, 2005.

[56] C. Zhang and D. Xing, "Miniaturized PCR chips for nucleic acid amplification and analysis: latest advances and future trends," *Nucleic Acids Research,* vol. 35, pp. 4223-4237, 2007.

[57] C. Iliescu, H. Taylor, M. Avram, J. Miao, and S. Franssila, "A practical guide for the fabrication of microfluidic devices using glass and silicon," *Biomicrofluidics,* vol. 6, p. 016505, 2012.

[58] S.-E. Ong, S. Zhang, H. Du, and Y. Fu, "Fundamental principles and applications of microfluidic systems," *Front Biosci,* vol. 13, pp. 2757-2773, 2008.

[59] D. A. Bartholomeusz, R. W. Boutté, and J. D. Andrade, "Xurography: rapid prototyping of microstructures using a cutting plotter," *Journal of Microelectromechanical Systems,* vol. 14, pp. 1364-1374, 2005.

[60] M. A. Shoffner, J. Cheng, G. E. Hvichia, L. J. Kricka, and P. Wilding, "Chip PCR. I. Surface passivation of microfabricated silicon-glass chips for PCR," *Nucleic Acids Research,* vol. 24, pp. 375-379, 1996.

[61] J. Cheng, M. A. Shoffner, G. E. Hvichia, L. J. Kricka, and P. Wilding, "Chip PCR. II. Investigation of different PCR amplification systems in microfabricated silicon-glass chips," *Nucleic Acids Research,* vol. 24, pp. 380-385, 1996.

[62] L. A. Legendre, J. M. Bienvenue, M. G. Roper, J. P. Ferrance, and J. P. Landers, "A simple, valveless microfluidic sample preparation device for extraction and amplification of DNA from nanoliter-volume samples," *Analytical chemistry,* vol. 78, pp. 1444-1451, 2006.

[63] D. Dressman, H. Yan, G. Traverso, K. W. Kinzler, and B. Vogelstein, "Transforming single DNA molecules into fluorescent magnetic particles for detection and enumeration of genetic variations," *Proceedings of the National Academy of Sciences,* vol. 100, pp. 8817-8822, 2003.

[64] T. Kojima, Y. Takei, M. Ohtsuka, Y. Kawarasaki, T. Yamane, and H. Nakano, "PCR amplification from single DNA molecules on magnetic beads in emulsion: application for high-throughput screening of transcription factor targets," *Nucleic acids research,* vol. 33, pp. e150-e150, 2005.

[65] P. Kumaresan, C. J. Yang, S. A. Cronier, R. G. Blazej, and R. A. Mathies, "High-throughput single copy DNA amplification and cell analysis in engineered nanoliter droplets," *Analytical chemistry,* vol. 80, pp. 3522-3529, 2008.

[66] A. Manz, N. Graber, and H. Widmer, "Miniaturized total chemical analysis systems: a novel concept for chemical sensing," *Sensors and actuators B: Chemical,* vol. 1, pp. 244-248, 1990.

[67] H. Tian, L. C. Brody, and J. P. Landers, "Rapid detection of deletion, insertion, and substitution mutations via heteroduplex analysis using capillary-and microchip-based electrophoresis," *Genome research,* vol. 10, pp. 1403-1413, 2000.

[68] Y. Hataoka, L. Zhang, T. Yukimasa, and Y. Baba, "Rapid microvolume PCR of DNA confirmed by microchip electrophoresis," *Analytical sciences,* vol. 21, pp. 53-56, 2005.

[69] M. Paidipalli, I. Pjescic, P. L. Hindmarsh, and N. D. Crews, "Single-Step Intercalating Dye Strategies for DNA Damage Studies," *Journal of Microbiological Methods,* 2013.

[70] A. X. Meng, F. Jalali, A. Cuddihy, N. Chan, R. S. Bindra, P. M. Glazer, and R. G. Bristow, "Hypoxia down-regulates DNA double strand break repair gene expression in prostate cancer cells," *Radiotherapy and oncology,* vol. 76, pp. 168-176, 2005.

[71] A. R. Collins, "The comet assay for DNA damage and repair," *Molecular biotechnology,* vol. 26, pp. 249-261, 2004.

[72] A. Wekhof, F.-J. Trompeter, and O. Franken, "Pulsed UV disintegration (PUVD): a new sterilisation mechanism for packaging and broad medical-hospital applications," in *The first international conference on ultraviolet technologies*, 2001, pp. 14-16.

[73] Y. Hidaka and K. Kubota, "Study on the sterilization of grain surface using UV radiation," *Japan Agricultural Research Quarterly,* vol. 40, pp. 157-161, 2006.

[74] B. F. Ozen and J. D. Floros, "Effects of emerging food processing techniques on the packaging materials," *Trends in Food Science & Technology,* vol. 12, pp. 60-67, 2001.

[75] B. R. Mohapatra and M. T. La Duc, "Rapid detection of viable Bacillus pumilus SAFR-032 encapsulated spores using novel propidium monoazide-linked fluorescence in situ hybridization," *Journal of microbiological methods,* vol. 90, pp. 15-19, 2012.

[76] E. Omiccioli, G. Amagliani, G. Brandi, and M. Magnani, "A new platform for Real-Time PCR detection of Salmonella spp., Listeria monocytogenes and Escherichia coli O157 in milk," *Food microbiology,* vol. 26, pp. 615-622, 2009.

[77] J. M. Winchell, B. J. Wolff, R. Tiller, M. D. Bowen, and A. R. Hoffmaster, "Rapid identification and discrimination of Brucella isolates by use of real-time PCR and high-resolution melt analysis," *Journal of clinical microbiology,* vol. 48, pp. 697-702, 2010.

[78] K. E. Templeton, S. A. Scheltinga, M. F. Beersma, A. C. Kroes, and E. C. Claas, "Rapid and sensitive method using multiplex real-time PCR for diagnosis of infections by influenza A and influenza B viruses, respiratory syncytial virus, and parainfluenza viruses 1, 2, 3, and 4," *Journal of clinical microbiology,* vol. 42, pp. 1564-1569, 2004.

[79] T. Morrison, J. Hurley, J. Garcia, K. Yoder, A. Katz, D. Roberts, J. Cho, T. Kanigan, S. E. Ilyin, and D. Horowitz, "Nanoliter high throughput quantitative PCR," *Nucleic acids research,* vol. 34, pp. e123-e123, 2006.

[80] A. Fekete, K. Módos, M. Hegedüs, G. Kovács, G. Rontó, Á. Péter, H. Lammer, and C. Panitz, "DNA damage under simulated extraterrestrial conditions in bacteriophage T7," *Advances in Space Research,* vol. 36, pp. 303-310, 2005.

[81] H. Yoshida and J. D. Regan, "Solar UVB dosimetry by amplification of short and long segments in phage LD DNA," *Photochemistry and photobiology,* vol. 66, pp. 672-675, 1997.

[82] F. E. Ahmed, "Detection of genetically modified organisms in foods," *TRENDS in Biotechnology,* vol. 20, pp. 215-223, 2002.

[83] C. Lee, J. Kim, S. G. Shin, and S. Hwang, "Absolute and relative QPCR quantification of plasmid copy number in Escherichia coli," *Journal of biotechnology,* vol. 123, pp. 273-280, 2006.

[84] C. L. Lee, D. S. W. Ow, and S. K. W. Oh, "Quantitative real-time polymerase chain reaction for determination of plasmid copy number in bacteria," *Journal of microbiological methods,* vol. 65, pp. 258-267, 2006.

[85] A. Rueckert, R. S. Ronimus, and H. W. Morgan, "Development of a rapid detection and enumeration method for thermophilic bacilli in milk powders," *Journal of microbiological methods,* vol. 60, pp. 155-167, 2005.

[86] R. H. Lipsky, C. M. Mazzanti, J. G. Rudolph, K. Xu, G. Vyas, D. Bozak, M. Q. Radel, and D. Goldman, "DNA melting analysis for detection of single nucleotide polymorphisms," *Clinical chemistry,* vol. 47, pp. 635-644, 2001.

[87] G. H. Reed, J. O. Kent, and C. T. Wittwer, "High-resolution DNA melting analysis for simple and efficient molecular diagnostics," *Pharmacogenomics,* vol. 8, pp. 597-608, 2007.

[88] L. Zhou, L. Wang, R. Palais, R. Pryor, and C. T. Wittwer, "High-resolution DNA melting analysis for simultaneous mutation scanning and genotyping in solution," *Clinical Chemistry,* vol. 51, pp. 1770-1777, 2005.

[89] R. H. Vossen, E. Aten, A. Roos, and J. T. den Dunnen, "High-Resolution Melting Analysis (HRMA)—More than just sequence variant screening," *Human mutation,* vol. 30, pp. 860-866, 2009.

[90] V. Andriantsoanirina, V. Lascombes, A. Ratsimbasoa, C. Bouchier, J. Hoffman, M. Tichit, L.-P. Rabarijaona, R. Durand, and D. Ménard, "Rapid detection of point mutations in Plasmodium falciparum genes associated with antimalarial drugs resistance by using High-Resolution Melting analysis," *Journal of microbiological methods,* vol. 78, pp. 165-170, 2009.

[91] A. Pangasa, A. R. Jex, B. E. Campbell, N. J. Bott, M. Whipp, G. Hogg, M. A. Stevens, and R. B. Gasser, "High resolution melting-curve (HRM) analysis for the diagnosis of cryptosporidiosis in humans," *Molecular and cellular probes,* vol. 23, pp. 10-15, 2009.

[92] C. T. Wittwer, G. H. Reed, C. N. Gundry, J. G. Vandersteen, and R. J. Pryor, "High-resolution genotyping by amplicon melting analysis using LCGreen," *Clinical chemistry,* vol. 49, pp. 853-860, 2003.

[93] M. G. Herrmann, J. D. Durtschi, C. T. Wittwer, and K. V. Voelkerding, "Expanded instrument comparison of amplicon DNA melting analysis for mutation scanning and genotyping," *Clinical chemistry,* vol. 53, pp. 1544-1548, 2007.

[94] V. Gurtler, D. Grando, B. C. Mayall, J. Wang, and S. Ghaly-Derias, "A novel method for simultaneous Enterococcus species identification/typing and van genotyping by high resolution melt analysis," *Journal of microbiological methods,* vol. 90, pp. 167-181, 2012.

[95] Z. Kuluncsics, D. Perdiz, E. Brulay, B. Muel, and E. Sage, "Wavelength dependence of ultraviolet-induced DNA damage distribution: involvement of direct or indirect mechanisms and possible artefacts," *Journal of Photochemistry and Photobiology B: Biology,* vol. 49, pp. 71-80, 1999.

[96] C. T. Wittwer, G. B. Reed, and K. M. Ririe, "Rapid Cycle DNA Amplification," in *The Polymerase Chain Reaction*, K. B. Mullis, F. Ferre, and R. Gibbs, Eds. Deerfield Beach: Springer-Verlag, 1994, pp. 174-181.

[97] T. Douki and J. Cadet, "Individual Determination of the Yield of the Main UV-Induced Dimeric Pyrimidine Photoproducts in DNA Suggests a High Mutagenicity of CC Photolesions " *Biochemistry,* vol. 40, pp. 2495-2501, 2001.

[98] K. J. Breslauer, R. Frank, H. Blöcker, and L. A. Marky, "Predicting DNA duplex stability from the base sequence," *Proceedings of the National Academy of Sciences,* vol. 83, pp. 3746-3750, 1986.

[99] J. SantaLucia, "A unified view of polymer, dumbbell, and oligonucleotide DNA nearest-neighbor thermodynamics," *Proceedings of the National Academy of Sciences,* vol. 95, pp. 1460-1465, 1998.

[100] C. Iliescu, J. Jing, F. E. Tay, J. Miao, and T. Sun, "Characterization of masking layers for deep wet etching of glass in an improved HF/HCl solution," *Surface and Coatings Technology,* vol. 198, pp. 314-318, 2005.

[101] C. Iliescu, F. E. Tay, and J. Miao, "Strategies in deep wet etching of Pyrex glass," *Sensors and Actuators A: Physical,* vol. 133, pp. 395-400, 2007.

[102] M. Howlader, S. Suehara, H. Takagi, T. Kim, R. Maeda, and T. Suga, "Room-temperature microfluidics packaging using sequential plasma activation process," *Advanced Packaging, IEEE Transactions on,* vol. 29, pp. 448-456, 2006.

[103] L. Xinghua, T. Abe, Y. Liu, and M. Esashi, "Fabrication of high-density electrical feed-throughs by deep-reactive-ion etching of Pyrex glass," *Journal of Microelectromechanical Systems,* vol. 11, pp. 625-630, 2002.

[104] K. Kolari, V. Saarela, and S. Franssila, "Deep plasma etching of glass for fluidic devices with different mask materials," *Journal of Micromechanics and Microengineering,* vol. 18, p. 064010, 2008.

[105] A. Baram and M. Naftali, "Dry etching of deep cavities in Pyrex for MEMS applications using standard lithography," *Journal of Micromechanics and Microengineering,* vol. 16, p. 2287, 2006.

[106] T. Akashi and Y. Yoshimura, "Deep reactive ion etching of borosilicate glass using an anodically bonded silicon wafer as an etching mask," *Journal of Micromechanics and Microengineering,* vol. 16, p. 1051, 2006.

[107] E. Thiénot, F. Domingo, E. Cambril, and C. Gosse, "Reactive ion etching of glass for biochip applications: Composition effects and surface damages," *Microelectronic engineering,* vol. 83, pp. 1155-1158, 2006.

[108] X. X. Zhang and J.-P. Raskin, "Low-temperature wafer bonding: a study of void formation and influence on bonding strength," *Journal of Microelectromechanical Systems, ,* vol. 14, pp. 368-382, 2005.

[109] P. Abgrall and A. Gue, "Lab-on-chip technologies: making a microfluidic network and coupling it into a complete microsystem—a review," *Journal of Micromechanics and Microengineering,* vol. 17, p. R15, 2007.

[110] P. Mao and J. Han, "Fabrication and characterization of 20 nm planar nanofluidic channels by glass–glass and glass–silicon bonding," *Lab on a Chip,* vol. 5, pp. 837-844, 2005.

[111] J. Wei, "Wafer bonding techniques for microsystem packaging," in *Journal of Physics: Conference Series*, 2006, p. 943.

[112] M. Howlader, S. Suehara, and T. Suga, "Room temperature wafer level glass/glass bonding," *Sensors and Actuators A: Physical,* vol. 127, pp. 31-36, 2006.

[113] Z.-J. Jia, Q. Fang, and Z.-L. Fang, "Bonding of glass microfluidic chips at room temperatures," *Analytical chemistry,* vol. 76, pp. 5597-5602, 2004.

[114] P. Mrozek, "Anodic bonding of glasses with interlayers for fully transparent device applications," *Sensors and Actuators A: Physical,* vol. 151, pp. 77-80, 2009.

[115] D. P. Poenar, C. Iliescu, M. Carp, A. J. Pang, and K. J. Leck, "Glass-based microfluidic device fabricated by Parylene wafer-to-wafer bonding for impedance spectroscopy," *Sensors and Actuators A: Physical,* vol. 139, pp. 162-171, 2007.

[116] C. Iliescu, D. P. Poenar, M. Carp, and F. C. Loe, "A microfluidic device for impedance spectroscopy analysis of biological samples," *Sensors and Actuators B: Chemical,* vol. 123, pp. 168-176, 2007.

[117] S. Metz, S. Jiguet, A. Bertsch, and P. Renaud, "Polyimide and SU-8 microfluidic devices manufactured by heat-depolymerizable sacrificial material technique," *Lab on a Chip,* vol. 4, pp. 114-120, 2004.

[118] M. Bu, T. Melvin, G. J. Ensell, J. S. Wilkinson, and A. G. Evans, "A new masking technology for deep glass etching and its microfluidic application," *Sensors and Actuators A: Physical,* vol. 115, pp. 476-482, 2004.

[119] A. Berthold, P. Sarro, and M. Vellekoop, "Two-step glass wet-etching for micro-fluidic devices," in *Proceedings of the SeSens workshop*, 2000.

[120] P. C. Simpson, A. T. Woolley, and R. A. Mathies, "Microfabrication technology for the production of capillary array electrophoresis chips," *Biomedical Microdevices,* vol. 1, pp. 7-26, 1998.

[121] C. Iliescu, J. Miao, and F. E. Tay, "Stress control in masking layers for deep wet micromachining of Pyrex glass," *Sensors and Actuators A: Physical,* vol. 117, pp. 286-292, 2005.

[122] F. E. Tay, C. Iliescu, J. Jing, and J. Miao, "Defect-free wet etching through Pyrex glass using Cr/Au mask," *Microsystem technologies,* vol. 12, pp. 935-939, 2006.

[123] C. Iliescu, B. Chen, and J. Miao, "Deep wet etching-through 1mm pyrex glass wafer for microfluidic applications," in *Micro Electro Mechanical Systems, 2007. MEMS. IEEE 20th International Conference on*, 2007, pp. 393-396.

[124] C.-H. Lin, G.-B. Lee, Y.-H. Lin, and G.-L. Chang, "A fast prototyping process for fabrication of microfluidic systems on soda-lime glass," *Journal of Micromechanics and Microengineering,* vol. 11, p. 726, 2001.

[125] N. Chiem, L. Lockyear-Shultz, P. Andersson, C. Skinner, and D. J. Harrison, "Room temperature bonding of micromachined glass devices for capillary electrophoresis," *Sensors and Actuators B: Chemical,* vol. 63, pp. 147-152, 2000.

[126] L. Chen, G. Luo, K. Liu, J. Ma, B. Yao, Y. Yan, and Y. Wang, "Bonding of glass-based microfluidic chips at low-or room-temperature in routine laboratory," *Sensors and Actuators B: Chemical,* vol. 119, pp. 335-344, 2006.

[127] M. Doms, H. Feindt, W. Kuipers, D. Shewtanasoontorn, A. Matar, S. Brinkhues, R. Welton, and J. Mueller, "Hydrophobic coatings for MEMS applications," *Journal of Micromechanics and Microengineering,* vol. 18, p. 055030, 2008.

[128] W. R. Ashurst, C. Yau, C. Carraro, R. Maboudian, and M. T. Dugger, "Dichlorodimethylsilane as an anti-stiction monolayer for MEMS: A comparison to the octadecyltrichlorosilane self-assembled monolayer," *Journal of Microelectromechanical Systems,* vol. 10, pp. 41-49, 2001.